

# A Stochastic Particle Variational Bayesian Inference Inspired Deep-Unfolding Network for Non-Convex Parameter Estimation

Zhixiang Hu, An Liu, *Senior Member, IEEE*, and Minjian Zhao, *Member, IEEE*

**Abstract**—Future wireless networks are envisioned to provide ubiquitous sensing services, which also gives rise to a substantial demand for high-dimensional non-convex parameter estimation, i.e., the associated likelihood function is non-convex and contains numerous local optima. Variational Bayesian inference (VBI) provides a powerful tool for modeling complex estimation problems and reasoning with prior information, but poses a long-standing challenge on computing intractable posteriori distributions. Most existing variational methods generally rely on assumptions about specific distribution families to derive closed-form solutions, and are difficult to apply in high-dimensional, non-convex scenarios. Given these challenges, firstly, we propose a parallel stochastic particle variational Bayesian inference (PSPVBI) algorithm. Thanks to innovations such as particle approximation, additional updates of particle positions, and parallel stochastic successive convex approximation (PSSCA), PSPVBI can flexibly drive particles to fit the posteriori distribution with acceptable complexity, yielding high-precision estimates of the target parameters. Furthermore, additional speedup can be obtained by deep-unfolding (DU) the PSPVBI algorithm. Specifically, superior hyperparameters are learned to dramatically reduce the number of algorithmic iterations. In this PSPVBI-induced Deep-Unfolding Networks, some techniques related to gradient computation, data sub-sampling, differentiable sampling, and generalization ability are also employed to facilitate the practical deployment. Finally, we apply the LPSPVBI to solve several important parameter estimation problems in wireless sensing scenarios. Simulations indicate that the LPSPVBI algorithm outperforms existing solutions.

**Index Terms**—Non-convex parameter estimation, variational Bayesian inference, deep-unfolding, particle approximation, stochastic successive convex approximation.

## I. INTRODUCTION

**F**UTURE multi-functional wireless networks envisioned by next-generation communication standards (e.g., 6G, Wi-Fi 7, and Wi-Fi 8) are not only an extension of existing communication technology but also are expected to provide various high-accuracy sensing services, such as indoor positioning, activity recognition, radar sensing, Integrated Sensing and Communications (ISAC) [1] and so on. These sensing services drive the need for accurate estimation of multi-target parameters such as distance, angle, and speed in complex wireless environment, which often involves high-dimensional non-convex parameter estimation problems. In this case, traditional parameter estimation methods such as Maximum Likelihood

(ML) estimation and Maximum-a-Posteriori (MAP) estimation can easily get trapped in a “bad” local optimum of the corresponding high-dimensional non-convex objective function. It is well known that Bayesian inference is more suitable for high-dimensional non-convex parameter estimation because of its powerful ability in exploiting prior information and modeling the uncertainty in parameters. Moreover, Bayesian inference can provide the entire posteriori distribution rather than a point estimate, so it is not easily trapped into local optimums. However, it casts a long-standing challenge on deriving intractable posteriori distributions. For most non-trivial models and real-world applications, multiple integrals in a posteriori distribution are impossible or very difficult to compute in closed form, so practitioners must resort to approximate methods.

The methods of approximate posteriori can be broadly divided into two categories, variational bayesian inference (VBI) [2], [3] and the Monte Carlo methods [4], [5], [6].

VBI can provide an analytical approximation to the posteriori distributions by iteratively updating the variational probability distributions to optimize Kullback-Leibler (KL) divergence. As a deterministic approximation, VBI can handle high-dimensional parameter spaces by selecting suitable optimization algorithms, so it is often scalable to large-scale data sets and complex models [7]. However, for the conventional VBI, it is usually assumed that the distributions come from certain special distribution families or satisfy conjugate conditions [8]. These assumptions are often not accurate enough and can be subjective. Simple distribution sets may not be flexible enough to fit a true posteriori distribution well, while more advanced choices pose difficulties for the subsequent optimization tasks. For this reason, efficient variational methods often need to be derived on a model-by-model basis, causing is a major barrier for developing general purpose algorithms.

In another line of research, the Monte Carlo method approximates a true posteriori by generating samples from distributions through sampling techniques such as Markov chain Monte Carlo (MCMC) [4], sequential Monte Carlo (SMC) [5], importance sampling (IS) [9], [6], etc. Therefore, the method can be more flexible in characterizing prior and posteriori distributions, so it can be applied to a variety of non-standard probability distributions and can be performed in parallel. However, such methods are generally slow and difficult to converge [7], and can also become inapplicable and inefficient in high-dimensional problems.

Further combining the advantages of the two methods,

Zhixiang Hu, An Liu and Minjian Zhao are with the College of Information Science and Electronic Engineering, Zhejiang University, Hangzhou 310027, China, e-mail: anliu@zju.edu.cn.

particle VBI (PVBI) came into being. The VBI framework ensures efficient probabilistic inference in PVBI, and the sampling technique employed makes it scalable to complex models. Some works have been done exploring this route. In [3], although discrete particles are used to fit the variational posteriori, conjugate prior assumptions are still adopted, which limits its scope of use. In [10], the method of particle mirror descent (PMD) updates only the weights of the particles, but not the positions of the particles. Although the other kernel-based PMD proposed in this paper can change the particle positions by resampling, the kernel-based method needs to deal with continuous multiple integrals, which will increase the complexity significantly and may further lead to weight degradation. In [7], with the theoretical guidance of functional analysis, Stein Variational Gradient Descent (SVGD) directly drives the particles to update their positions, and finally approximates the posteriori distribution according to the statistics of the aggregated particles. However, when there are many variables and with a wide range of values, this approach becomes unacceptably complex. An inappropriate kernel function can also result in degraded performance of the SVGD. In order to further improve the approximate efficiency of the particles and reduce the number of particles used in PVBI, we decided to update both the weights and positions of the particles to directly minimize the KL divergence. Such improved degree of freedom can further enhance the performance and accelerate the convergence speed.

In addition, for high-dimensional problems, the volume of sample space increases exponentially, and effectively covering this large sample space requires a large number of samples. The challenge of such a dimensional disaster also requires PVBI to deal with. In [8], [11], stochastic optimization is employed to optimize the variational objective function in the VBI, where a fast noisy approximation of the gradient is calculated from Monte Carlo samples from the variational distribution. With certain conditions on the step-size schedule, the noisy estimates of a gradient guarantee these algorithms can provably converge to an optimum, which are often cheaper to compute than the true gradient. On this basis, we refer to stochastic successive convex approximation (SSCA) [12], [13] and propose a novel stochastic particle variational Bayesian inference (SPVBI) algorithm in [14] for the special case of multiband sensing problem. The algorithm takes an average in both gradient and iterates (optimization variables) with decreasing step sizes, and updates optimization variables alternatively by solving a sequence of convex surrogate subproblems. In summary, SPVBI algorithm combines variational Bayesian inference, Monte Carlo sampling, stochastic optimization to give full play to their respective advantages. However, the SPVBI in [14] is specifically designed for multiband sensing. Moreover, although the convergence can be guaranteed by alternating optimization with the decreasing step sizes, the convergence speed is still slow especially for high-dimensional problems.

Most practical parameter estimation applications require immediate results in the case of low latency and limited complexity, which implies that algorithms can afford only a very small number of iterations (e.g., ten or fewer) [15], [16].

In order to accelerate the convergence speed, it is necessary to carefully tune the hyperparameters (e.g., step-size selection), which is heuristic and not reliable. To solve this problem, a model-driven deep learning scheme, deep unfolding (DU), has been proposed recently. The main idea of DU is to unfold the iterative algorithm as a series of neural network layers with some learnable parameters. Although there are currently some VBI-inspired DU networks [17], [18], [19], they are all based on conventional VBI algorithms and are heavily constrained by distribution assumptions and application scenarios, thus exhibiting obvious limitations. In addition, for the process of unfolding SPVBI algorithm, a series of challenges still need to be overcome, such as the feasibility of network backpropagation, the generalization ability and so on.

In this paper, we propose a parallel stochastic particle variational Bayesian inference (PSPVBI) algorithm, which can be viewed as an extension of the SPVBI in [14] from multiband sensing to more general parameter estimation scenes, and from alternating optimization to parallel optimization to facilitate deep unfolding and convergence acceleration. In addition, we deep-unfold PSPVBI to derive a learnable PSPVBI (LPSPVBI) algorithm to further reduce the complexity. The main contributions are summarized below.

- **A parallel stochastic particle VBI method and its convergence proof.** The proposed PSPVBI algorithm combines the advantages of variational inference and Monte Carlo sampling to approximate the posteriori probability distribution, and can describe various prior and posteriori distributions flexibly and efficiently, and can also be applied to high-dimensional non-convex problems. Updating particle weights and particle positions simultaneously reduces the number of required particles and speeds up convergence. In addition, we introduce parallel stochastic successive convex approximations (PSSCA) to deal with the tricky crux of Bayesian inference regarding multiple integrals. Different from stochastic VBI (SVBI) [11], we average the gradient at the same time as the iterates, which makes the noisy estimates of gradient smooth continuously with the iteration, and also provides convergence guarantee for the algorithm.
- **Learnable PSPVBI greatly accelerating convergence and reducing computational complexity.** By fusing the PSPVBI algorithm that have performance guarantees with tools from deep learning, key hyperparameters in the principled algorithm can be learned, greatly accelerating convergence and reducing overall algorithm complexity. Existing performance guarantees for the original PSPVBI algorithm can apply verbatim to learned unfolded networks and appropriate constraints can be imposed on the learned parameters. The resulting unfolded algorithm is intuitive, interpretable, and has low complexity and memory requirements, which is in stark contrast to black-box NNs.
- **Specific deep-unfolding algorithm design for actual deployment.** We apply the LPSPVBI to solve several important application problems on parameter estimation in sensing scenes. Simulation results show that the proposed

LPSPVBI algorithm achieves competitive performance for both scenes. For deployment details, we also provided some practical tricks. For example, HyperNet [20], [21] is used to improve the generalization ability of deep unfolding network, sharing intermediate computation results and subsampling observed data are used to reduce the cost of computing gradients, and deep neural network (DNN) is used to fit the sampling process to make sampling efficient and backpropagated.

The rest of the paper is organized as follows. The general problem formulation is given in Section II, together with two application examples. The PSPVBI algorithm and the convergence analysis are presented in Section III. The learnable PSPVBI algorithm is proposed in Section IV. In Section V, we present numerical simulations and performance analysis. Section VI applies the LPSPVBI algorithm to solve several important application problems. Finally, conclusions are given in Section VII.

Notations:  $\delta(\cdot)$  denotes the Dirac's delta function,  $vec[\cdot]$  denotes the vectorization operation,  $\propto$  denotes the left is proportional to the right,  $\text{Re}(\cdot)$  denotes the real part operator,  $\text{var}(\cdot)$  denotes the variance operator, and  $\|\cdot\|$  denotes the Euclidean norm. For a matrix  $\mathbf{A}$ ,  $\mathbf{A}^T$ ,  $\mathbf{A}^H$ ,  $\mathbf{A}^{-1}$ , represent a transpose, complex conjugate transpose and inverse, respectively.  $\mathbb{E}_z[\cdot]$  denotes the expectation operator with respect to the random vector  $z$ .  $\mathbf{D}_{KL}[q||p]$  denotes the Kullback-Leibler (KL) divergence of the probability distributions  $q$  and  $p$ .  $\mathcal{N}(\mu, \Sigma)$  and  $\mathcal{CN}(\mu, \Sigma)$  denotes Gaussian and complex Gaussian distribution with mean  $\mu$  and covariance matrix  $\Sigma$ .

## II. GENERAL PROBLEM FORMULATION FOR NON-CONVEX PARAMETER ESTIMATION

Consider the following general measurement model of non-convex parameter estimation:

$$r_n = f_n(\boldsymbol{\theta}) + w_n, \forall n = 1, 2, \dots, N, \quad (1)$$

where  $r_n$  denotes the  $n$ -th observed data,  $N$  is the total number of observations, and  $w_n$  denotes an additive white Gaussian noise (AWGN) following the distribution  $\mathcal{CN}(0, \eta_w^2)$ . The variables to be estimated are denoted as  $\boldsymbol{\theta} = [\theta_1, \dots, \theta_J]^T$ , and  $J$  is the number of variables.  $f_n(\boldsymbol{\theta})$  is defined as the measurement function reconstructed from the parameters  $\boldsymbol{\theta}$ .

All observed data can be vectorized as  $\mathbf{r} = [r_1, r_2, \dots, r_N]^T$ . In the case of AWGN, the likelihood function of the measurement model can be written as follow

$$p(\mathbf{r}|\boldsymbol{\theta}) = \prod_{n=1}^N p(r_n|\boldsymbol{\theta}) = \prod_{n=1}^N \frac{1}{\sqrt{2\pi}\eta_w} \exp\left(\frac{|r_n - f_n(\boldsymbol{\theta})|^2}{-2\eta_w^2}\right). \quad (2)$$

The key step in Bayesian inference is to obtain the posteriori distribution, denoted by  $p(\boldsymbol{\theta}|\mathbf{r})$ . Following the Bayes' theorem, the posteriori distribution of the unknown parameters is  $p(\boldsymbol{\theta}|\mathbf{r}) \propto p(\mathbf{r}|\boldsymbol{\theta})p(\boldsymbol{\theta})$ , where  $p(\boldsymbol{\theta})$  denotes the potential prior distribution. For a variable  $\theta_j$  of interest, the marginal posteriori distribution is denoted as

$$p(\theta_j|\mathbf{r}) \propto \int p(\mathbf{r}|\boldsymbol{\theta})p(\boldsymbol{\theta})d\boldsymbol{\theta}_{\sim j}, \quad (3)$$

where  $\boldsymbol{\theta}_{\sim j}$  represents all the other variables except  $\theta_j$ . Generally, it is intractable to get a closed-form solution for  $p(\theta_j|\mathbf{r})$  due to the high dimensional integrals over  $\boldsymbol{\theta}_{\sim j}$  and complicated measurement functions  $f_n(\boldsymbol{\theta})$ .

VBI casts the posteriori inference as an optimization problem, where variational distributions  $q(\boldsymbol{\theta})$  are adjusted to approximate the true posteriori distributions  $p(\boldsymbol{\theta}|\mathbf{r})$ . The closeness is measured with Kullback-Leibler divergence, which is defined as

$$\begin{aligned} \mathbf{D}_{KL}[q||p] &= \int q(\boldsymbol{\theta}) \ln \frac{q(\boldsymbol{\theta})}{p(\boldsymbol{\theta}|\mathbf{r})} d\boldsymbol{\theta} \\ &= \int q(\boldsymbol{\theta}) \ln \frac{q(\boldsymbol{\theta})p(\mathbf{r})}{p(\mathbf{r}|\boldsymbol{\theta})p(\boldsymbol{\theta})} d\boldsymbol{\theta}, \end{aligned} \quad (4)$$

where  $q(\boldsymbol{\theta})$  is assumed to be factorized as [2], [22]  $q(\boldsymbol{\theta}) = \prod_{j=1}^J q(\theta_j)$ , where  $q(\theta_j)$  stands for the approximation to the marginal posteriori  $p(\theta_j|\mathbf{r})$ .

Considering that  $p(\mathbf{r})$  is a constant independent of  $q(\boldsymbol{\theta})$ , minimizing the KL divergence is equivalent to solving the following optimization problem:

$$\mathcal{P}_1 : \boldsymbol{\theta}^* = \arg \min_q \int q(\boldsymbol{\theta}) \ln \frac{q(\boldsymbol{\theta})}{p(\mathbf{r}|\boldsymbol{\theta})p(\boldsymbol{\theta})} d\boldsymbol{\theta}. \quad (5)$$

In the following, we give some important application examples of the problem formulation in (5).

**Example 1.** (Wireless cooperative localization [6]). Consider a two-dimensional static wireless network, wherein the location-aware nodes are assumed to be uniformly distributed within the deployment area, as illustrated in Fig. 1. For a target node, there are  $N_R$  reference nodes in its measurement range  $r_s$ , whose initial locations are assumed to be inaccurate, due to errors in coarse acquisition. Moreover, the absence of anchors throughout the entire area necessitates collaborative localization efforts among the nodes themselves. The true (but unknown) position vectors of the target node and the  $i$ -th reference node are denoted as  $\mathbf{s}_0 = [px_0, py_0]^T$  and  $\mathbf{s}_i = [px_i, py_i]^T$ ,  $\forall i = 1, \dots, N_R$ , respectively, while the coarse locations (with a precision  $\mathbf{U}_i$ ,  $\forall i = 0, 1, \dots, N_R$ ) are denoted as  $\boldsymbol{\mu}_i$ ,  $\forall i = 0, 1, \dots, N_R$ . In general, the true location  $\mathbf{s}_i$ ,  $\forall i = 0, 1, \dots, N_R$ , can be modeled as Gaussian variables [23], characterized by a mean of  $\boldsymbol{\mu}_i$  and precision  $\mathbf{U}_i$ ,  $\mathbf{s}_i \sim \mathcal{N}(\boldsymbol{\mu}_i, \mathbf{U}_i)$ ,  $\forall i = 0, 1, \dots, N_R$ , where we assume node coarse locations and precisions are independent to each other [24], [25]. The prior information  $\boldsymbol{\mu}_i$  and  $\mathbf{U}_i$  recorded by each node, together with the measurement  $\mathbf{z}_i$ ,  $\forall i = 1, \dots, N_R$  between the target node and the reference nodes, are shared with the target node for cooperative localization.

The measurement model can be given by

$$\mathbf{z}_i = h(\mathbf{s}_i, \mathbf{s}_0) + \varepsilon_i, \forall i = 1, \dots, N_R, \quad (6)$$

where  $h(\mathbf{s}_i, \mathbf{s}_0)$  denotes the measurement function, and  $\varepsilon_i$  represents the measurement noise following the distribution  $\mathcal{N}(0, U_{ni})$ , where  $U_{ni}$  is the precision parameter. Specifically, this example adopt the received signal strength (RSS)-based measurement function, which is

$$h(\mathbf{s}_i, \mathbf{s}_0) = \phi_{\text{ref}} - 10\lambda \log_{10} \|\mathbf{s}_i - \mathbf{s}_0\|_2, \quad (7)$$

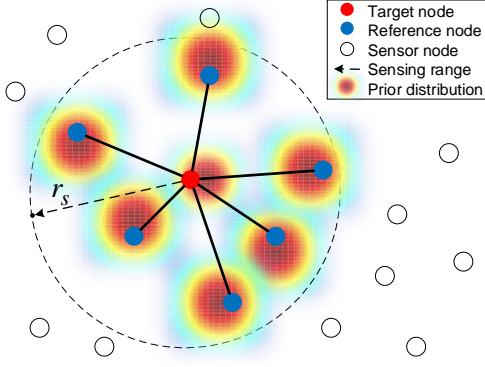


Fig. 1. Illustration of the network node deployment.

where  $\phi_{ref}$  denotes the reference power loss and  $\lambda$  denotes the path loss exponent [6]. Let  $\mathbf{c} = \text{vec}[\mathbf{s}_i]_{i=1}^{N_R}$  denote the reference node cluster of the target node, and  $\mathbf{z}_i$  are stacked as  $\mathbf{z} = \text{vec}[\mathbf{z}_i]_{i=1}^{N_R}$ . Under such a measurement model, the likelihood function can be written as follow

$$p(\mathbf{z}|\mathbf{s}_0, \mathbf{c}) = \prod_{i=1}^{N_R} \frac{|U_{ni}|^{\frac{1}{2}}}{\sqrt{2\pi}} \exp\left[-\frac{U_{ni}}{2} (\mathbf{z}_i - h(\mathbf{s}_i, \mathbf{s}_0))^2\right], \quad (8)$$

and the posteriori distribution is cast as

$$p(\mathbf{s}_i|\mathbf{z}) \propto \mathcal{N}(\boldsymbol{\mu}_0, \mathbf{U}_0) \cdot \prod_{i=1}^{N_R} \mathcal{N}(\boldsymbol{\mu}_i, \mathbf{U}_i) \cdot \int \frac{|U_{ni}|^{\frac{1}{2}}}{\sqrt{2\pi}} \exp\left[-\frac{1}{2} U_{ni} (\mathbf{z}_i - h(\mathbf{s}_i, \mathbf{s}_0))^2\right] d\mathbf{s}_i. \quad (9)$$

Due to the nonlinear measurement function (7) and reference node location errors, the posteriori distribution of the target node is non-convex and has many bad local optimums [6], which complicates the determination of the optimal target node location.

**Example 2.** (Multiband WiFi sensing [14], [26]). In the scene of multiband WiFi sensing, we consider a single-input single-output (SISO) system that uses OFDM training signals over  $M$  frequency subbands to estimate range between the mobile node and Wi-Fi device. The discrete received signal model in frequency domain can be formulated as [26]

$$r_m^{(n)} = \sum_{k=1}^K \alpha_k e^{j\beta_k} e^{-j2\pi(f_{c,m} + n f_{s,m})(\tau_k + \delta_m)} e^{j\phi_m} + w_m^{(n)}, \quad (10)$$

where  $m = 1, 2, \dots, M$  is the frequency band index,  $N_m$  denotes the number of subcarriers in each band,  $n = 0, 1, \dots, N_m - 1$  denotes subcarrier index and  $k = 1, 2, \dots, K$  denotes the  $k$ -th scattering path.  $\alpha_k e^{j\beta_k}$  is a complex scalar carrying the amplitude and phase information of a scattering path, and  $\tau_k$  is the time delay of the  $k$ -th path.  $f_{c,m}$  and  $f_{s,m}$  are the initial frequency and subcarrier spacing of  $m$ -th frequency band, respectively. In addition, due to the hardware imperfection, the CSI measurements are superimposed with a

random initial phase  $\phi_m$  and a timing synchronization error  $\delta_m$ .  $w_m^{(n)}$  denotes an additive white Gaussian noise (AWGN) following the distribution  $\mathcal{CN}(0, \eta_w^2)$ .

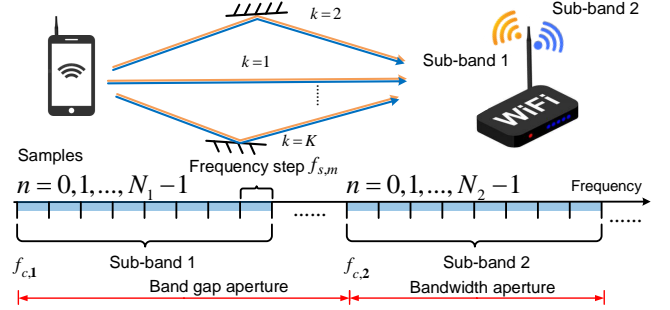


Fig. 2. Illustration of the multiband WiFi sensing.

In this case, the variables to be estimated are denoted as  $\boldsymbol{\Lambda}_{\text{ori}} = [\alpha_1, \dots, \alpha_K, \tau_1, \dots, \tau_K, \beta_1, \dots, \beta_K, \phi_1, \dots, \phi_M, \delta_1, \dots, \delta_M]^T$ , and frequency domain measurements of the received signal is vectorized as  $\mathbf{r} = [r_1^{(0)}, r_1^{(1)}, \dots, r_1^{(N_1-1)}, \dots, r_M^{(0)}, r_M^{(1)}, \dots, r_M^{(N_M-1)}]^T$ . In the case of AWGN, the logarithmic likelihood function of the original signal model (10) can be written as follow

$$\begin{aligned} \ln p(\mathbf{r}|\boldsymbol{\Lambda}_{\text{ori}}) &= \ln \prod_{m=1}^M \prod_{n=0}^{N_m-1} p(r_m^{(n)}|\boldsymbol{\Lambda}_{\text{ori}}) \\ &= MN_m \ln \frac{1}{\sqrt{2\pi\eta_w}} - \sum_{m=1}^M \sum_{n=0}^{N_m-1} \frac{1}{2\eta_w^2} \left| r_m^{(n)} - s_m^{(n)}(\boldsymbol{\Lambda}_{\text{ori}}) \right|^2, \end{aligned} \quad (11)$$

$$s_m^{(n)}(\boldsymbol{\Lambda}_{\text{ori}}) = \sum_{k=1}^K \alpha_k e^{j\beta_k} e^{-j2\pi(f_{c,m} + n f_{s,m})(\tau_k + \delta_m)} e^{j\phi_m}, \quad (12)$$

where  $s_m^{(n)}(\boldsymbol{\Lambda}_{\text{ori}})$  is the received signal reconstructed from the parameter  $\boldsymbol{\Lambda}_{\text{ori}}$ .

In the next section, we shall propose a general Bayesian algorithm to obtain the efficient approximation of marginal posteriori for the target parameters.

### III. PARALLEL STOCHASTIC PARTICLE VARIATIONAL BAYESIAN INFERENCE FOR NON-CONVEX PARAMETER ESTIMATION

#### A. Problem Formulation for PSPVBI

Since Problem  $\mathcal{P}_1$  is, in general, non-convex, we focus on designing an efficient algorithm to find a stationary point of  $\mathcal{P}_1$ . There are two major challenges in solving Problem  $\mathcal{P}_1$ : 1) there are generally many 'bad' local optimums in the objective function due to the non-convexity and high-dimension of the associated likelihood function; 2) it is difficult to obtain a marginal posteriori distribution of the target parameter, due to complex calculations of multiple integrals and tricky unstructured distribution assumptions.

We propose a parallel stochastic particle variational Bayesian inference (PSPVBI) algorithm to solve Problem  $\mathcal{P}_1$ , where variational posteriori probability  $q(\boldsymbol{\theta}_j)$

is approximated [3], [10] by a variational particle set  $\{p_{j,n}, w_{j,n} | \forall n = 1, \dots, N_p\}$  as follows

$$q(\boldsymbol{\theta}_j; \mathbf{p}_j, \mathbf{w}_j) = \sum_{n=1}^{N_p} w_{j,n} \delta(\boldsymbol{\theta}_j - p_{j,n}), \quad (13)$$

where  $N_p$  denotes the number of particles.  $\mathbf{p}_j = [p_{j,1}, p_{j,2}, \dots, p_{j,N_p}]^T$  and  $\mathbf{w}_j = [w_{j,1}, w_{j,2}, \dots, w_{j,N_p}]^T$  are the positions (i.e. supporting point) and weights of the particles, respectively. Particle positions can be initially drawn from a prior  $p_{j,n}^{(0)} \sim p(\boldsymbol{\theta}_j), \forall j, n$ , and the initial weights can be set to be uniform,  $w_{j,n}^{(0)} = \frac{1}{N_p}, \forall j, n$ . Compared with structured continuous distribution assumptions (e.g. Gaussian distribution, Gamma distribution, etc.), discrete particle sets consisting of positions and weights can efficiently describe the statistical probabilities of various variables within a given region. In addition, they can also provide globally optimal posteriori estimates and their associated belief compared to point estimates.

Given the particle approximation, we reformulate  $\mathcal{P}_1$  to the following optimization problem  $\mathcal{P}_2$ :

$$\begin{aligned} \mathcal{P}_2 : \min_{\mathbf{p}, \mathbf{w}} \quad & \mathbf{L}(\mathbf{p}, \mathbf{w}) \triangleq \int q(\boldsymbol{\theta}; \mathbf{p}, \mathbf{w}) \ln \frac{q(\boldsymbol{\theta}; \mathbf{p}, \mathbf{w})}{p(\mathbf{r}|\boldsymbol{\theta})p(\boldsymbol{\theta})} d\boldsymbol{\theta} \\ \text{s.t.} \quad & \sum_{n=1}^{N_p} w_{j,n} = 1, \quad \epsilon \leq w_{j,n} \leq 1, \quad \forall j, n, \\ & \hat{\boldsymbol{\theta}}_j - \Delta \hat{\boldsymbol{\theta}}_j / 2 \leq p_{j,n} \leq \hat{\boldsymbol{\theta}}_j + \Delta \hat{\boldsymbol{\theta}}_j / 2, \quad \forall j, n, \end{aligned}$$

where  $\epsilon > 0$  is a small number.  $\hat{\boldsymbol{\theta}}_j$  is the mean of the prior  $p(\boldsymbol{\theta}_j)$  and  $\Delta \hat{\boldsymbol{\theta}}_j$  is the range determined by the prior  $p(\boldsymbol{\theta}_j)$ . The truth value is highly likely to be located in the prior interval  $[\hat{\boldsymbol{\theta}}_j - \Delta \hat{\boldsymbol{\theta}}_j / 2, \hat{\boldsymbol{\theta}}_j + \Delta \hat{\boldsymbol{\theta}}_j / 2]$ , so the particle position is searched wherein to accelerate the convergence rate. Note that it does not make sense to generate particles with very small probabilities in approximate posteriori since these particles contribute very little to the estimator. Therefore, we restrict the probability of each particle  $w_{j,n}$  to be larger than a small number  $\epsilon$ .

In conventional PVBI, the position of particles are not updated. Besides, a large number of particles are required to overcome the instability caused by initial random sampling, and ensure that the estimation locally converges to a 'good' stationary point. As such, the complexity will rocket as the number of variables and particles increases.

Motivated by this observation, we optimize the particle position as well and further design an PSPVBI algorithm to solve the new problem with much lower per-iteration complexity than the conventional PVBI algorithm. Adding the optimization of particle positions  $\mathbf{p}$  can improve the effectiveness of characterizing the target distribution by discrete particles, and avoid the estimation result falling into the local optimum due to poor initial sampling. Furthermore, updating particle position can reduce the number of required particles, and thus effectively reduce the computational overhead, which will be discussed in detail in the following sections.

## B. PSPVBI Algorithm Design based on Parallel SSCA

Although updating particle positions can speed up convergence, multiple integration in the objective function  $\mathbf{L}(\mathbf{p}, \mathbf{w})$  of  $\mathcal{P}_2$  is still intractable. To solve this problem, we introduce the parallel stochastic successive convex approximations (PSSCA) [12], [13] to deal with the tricky crux of Bayesian inference regarding multiple integrals.

According to the mean field theory [22], the approximate posteriori probability of each variable can be assumed to be independent of each other, i.e.  $q(\boldsymbol{\theta}; \mathbf{p}, \mathbf{w}) = \prod_{j=1}^J q(\boldsymbol{\theta}_j; \mathbf{p}_j, \mathbf{w}_j)$ , so we have

$$\begin{aligned} \int q(\boldsymbol{\theta}) \ln q(\boldsymbol{\theta}) d\boldsymbol{\theta} &= \sum_{j=1}^J \int q(\boldsymbol{\theta}_j) \ln q(\boldsymbol{\theta}_j) d\boldsymbol{\theta}_j \\ &= \sum_{j=1}^J \sum_{n_j=1}^{N_p} w_{j,n_j} \ln w_{j,n_j} \triangleq C(\mathbf{w}). \end{aligned} \quad (14)$$

We shall use  $q(\boldsymbol{\theta})$  as a simplified notation for  $q(\boldsymbol{\theta}; \mathbf{p}, \mathbf{w})$ . Further for the objective function:

$$\begin{aligned} \mathbf{L}(\mathbf{p}, \mathbf{w}) &= \sum_{j=1}^J \int q(\boldsymbol{\theta}_j) \ln q(\boldsymbol{\theta}_j) d\boldsymbol{\theta}_j - \int q(\boldsymbol{\theta}) [\ln p(\mathbf{r}|\boldsymbol{\theta}) p(\boldsymbol{\theta})] d\boldsymbol{\theta} \\ &= C(\mathbf{w}) - \sum_{n_1=1}^{N_p} \dots \sum_{n_J=1}^{N_p} \tilde{w} [\ln p(\mathbf{r}|\boldsymbol{\theta}) + \ln p(\boldsymbol{\theta})] \Bigg|_{\boldsymbol{\theta}=\tilde{\mathbf{p}}}, \end{aligned} \quad (15)$$

where  $\tilde{w} = \prod_{j=1}^J w_{j,n_j}$  and  $\tilde{\mathbf{p}} = [p_{1,n_1}, \dots, p_{j,n_j}, \dots, p_{J,n_J}]^T$ . As you can see, the second part of (15) involves a summation of  $N_p^J$  terms. Therefore, it is unacceptable to directly solve  $\mathcal{P}_2$  due to its exponential complexity.

To overcome this challenge, we rewrite the objective function as

$$\mathbf{L}(\mathbf{p}, \mathbf{w}) = \mathbb{E}_{q(\boldsymbol{\theta})} [g(\mathbf{p}, \mathbf{w}; \boldsymbol{\theta})],$$

where  $\mathbb{E}_{q(\boldsymbol{\theta})} [\cdot]$  represents the expectation operator over the variational distribution  $q(\boldsymbol{\theta})$ , and  $g(\mathbf{p}, \mathbf{w}; \boldsymbol{\theta}) = C(\mathbf{w}) - [\ln p(\mathbf{r}|\boldsymbol{\theta}) + \ln p(\boldsymbol{\theta})]$ . Therefore,  $\mathcal{P}_2$  can be viewed as a stochastic optimization problem that involves a decision-dependent distribution, meaning that the random state  $\boldsymbol{\theta}$  follows the distribution  $q(\boldsymbol{\theta}; \mathbf{p}, \mathbf{w})$ , which depends on the value of the optimization variables  $\mathbf{p}, \mathbf{w}$ . We shall use  $q^{(t)}(\boldsymbol{\theta})$  as a simplified notation for  $q(\boldsymbol{\theta}; \mathbf{p}^{(t)}, \mathbf{w}^{(t)})$  in the  $t$ -th iteration.

For SSCA applied in the stochastic optimization [12], the basic idea behind it is to iteratively optimize a sequence of convex objective function (i.e. surrogate function) to approximate the original non-convex one. To update the particle position  $\mathbf{p}_j$  and particle weight  $\mathbf{w}_j$  of the  $j$ -th variable  $\boldsymbol{\theta}_j$ , we can choose quadratic convex functions [13], [12] as the surrogate objective functions

$$\bar{f}_{p_j}^{(t)}(\mathbf{p}_j) = \left(\mathbf{f}_{p_j}^{(t)}\right)^T \left(\mathbf{p}_j - \mathbf{p}_j^{(t)}\right) + \Gamma_{p_j}^{(t)} \left\| \mathbf{p}_j - \mathbf{p}_j^{(t)} \right\|^2, \quad (16)$$

$$\bar{f}_{w_j}^{(t)}(\mathbf{w}_j) = \left(\mathbf{f}_{w_j}^{(t)}\right)^T \left(\mathbf{w}_j - \mathbf{w}_j^{(t)}\right) + \Gamma_{w_j}^{(t)} \left\| \mathbf{w}_j - \mathbf{w}_j^{(t)} \right\|^2, \quad (17)$$

where  $\mathbf{f}_{p_j}^{(t)}$  and  $\mathbf{f}_{w_j}^{(t)}$  are unbiased estimators of the gradient  $\nabla_{\mathbf{p}_j} \mathbf{L}(\mathbf{p}^{(t)}, \mathbf{w}^{(t)})$  and  $\nabla_{\mathbf{w}_j} \mathbf{L}(\mathbf{p}^{(t)}, \mathbf{w}^{(t)})$ ,  $\Gamma_{p_j}^{(t)}$  and  $\Gamma_{w_j}^{(t)}$  are appropriately chosen positive stepsize. These surrogate sub-problems have closed-form solutions, which can be interpreted as the outcome of gradient projection [13], [14]. Therefore, we can obtain intermediate variables  $\bar{\mathbf{p}}_j^{(t)}, \bar{\mathbf{w}}_j^{(t)}$  by gradient projection as

$$\bar{\mathbf{p}}_j^{(t)} = Proj_{\Delta p} \left( \mathbf{p}_j^{(t)} - \Gamma_{p_j}^{(t)} \mathbf{f}_{p_j}^{(t)} \right), \quad (18)$$

$$\bar{\mathbf{w}}_j^{(t)} = Proj_{\Delta w} \left( \mathbf{w}_j^{(t)} - \Gamma_{w_j}^{(t)} \mathbf{f}_{w_j}^{(t)} \right), \quad (19)$$

where  $Proj_{\Delta p/\Delta w}(\cdot)$  denotes the projection operator related to the constraints in  $\mathcal{P}_2$ , which constrains particle positions and weights within a priori interval or a simplex and will be discussed in Section IV-A. Finally, the updated  $\{\mathbf{p}_j^{(t+1)}, \mathbf{w}_j^{(t+1)}\}, \forall j$  are given by

$$\mathbf{p}_j^{(t+1)} = (1 - \gamma^{(t)}) \mathbf{p}_j^{(t)} + \gamma^{(t)} \bar{\mathbf{p}}_j^{(t)}, \quad (20)$$

$$\mathbf{w}_j^{(t+1)} = (1 - \gamma^{(t)}) \mathbf{w}_j^{(t)} + \gamma^{(t)} \bar{\mathbf{w}}_j^{(t)}, \quad (21)$$

where  $\gamma^{(t)}$  is a decreasing step size that will be discussed later.

Next, we will give the construction of the unbiased estimators (i.e.  $\mathbf{f}_{p_j}^{(t)}$  and  $\mathbf{f}_{w_j}^{(t)}$ ) for the gradient of the objective function. The gradient of the objective function can be converted to the following form:

$$\nabla_{\mathbf{p}_j} \mathbf{L}(\mathbf{p}^{(t)}, \mathbf{w}^{(t)}) = \mathbb{E}_{q^{(t)}(\boldsymbol{\theta}_{\sim j})} \left[ \nabla_{\mathbf{p}_j} g_j \left( \mathbf{p}_j^{(t)}, \mathbf{w}_j^{(t)}; \boldsymbol{\theta}_{\sim j} \right) \right], \quad (22)$$

$$\nabla_{\mathbf{w}_j} \mathbf{L}(\mathbf{p}^{(t)}, \mathbf{w}^{(t)}) = \mathbb{E}_{q^{(t)}(\boldsymbol{\theta}_{\sim j})} \left[ \nabla_{\mathbf{w}_j} g_j \left( \mathbf{p}_j^{(t)}, \mathbf{w}_j^{(t)}; \boldsymbol{\theta}_{\sim j} \right) \right] \quad (23)$$

where

$$g_j(\mathbf{p}_j, \mathbf{w}_j; \boldsymbol{\theta}_{\sim j}) = C(\mathbf{w}) - \sum_{n_j=1}^{N_p} w_{j,n_j} \times \left[ \ln p(p_{j,n_j}) + \ln p(\mathbf{r} | \boldsymbol{\theta}_{\sim j}, p_{j,n_j}) \right], \quad (24)$$

and  $\boldsymbol{\theta}_{\sim j}$  represents all the other variables except  $\boldsymbol{\theta}_j$ .

To approximate the gradients in (22) and (23), in each iteration, based on the multiple samples of system state  $\boldsymbol{\theta}$  generated by the distribution  $q^{(t)}(\boldsymbol{\theta})$ ,  $\mathbf{f}_{p_j}^{(t)}$  and  $\mathbf{f}_{w_j}^{(t)}$  can be updated recursively as follows:

$$\mathbf{f}_{p_j}^{(t)} = (1 - \rho^{(t)}) \mathbf{f}_{p_j}^{(t-1)} + \frac{\rho^{(t)}}{B} \sum_{b=1}^B \nabla_{\mathbf{p}_j} g_j^{(t,b)}, \quad (25)$$

$$\mathbf{f}_{w_j}^{(t)} = (1 - \rho^{(t)}) \mathbf{f}_{w_j}^{(t-1)} + \frac{\rho^{(t)}}{B} \sum_{b=1}^B \nabla_{\mathbf{w}_j} g_j^{(t,b)}, \quad (26)$$

where

$$\begin{aligned} \nabla_{\mathbf{p}_j} g_j^{(t,b)} &= \nabla_{\mathbf{p}_j} g_j \left( \mathbf{p}_j, \mathbf{w}_j^{(t)}; \boldsymbol{\theta}_{\sim j}^{(b)} \right) \Big|_{\mathbf{p}_j = \mathbf{p}_j^{(t)}} \\ &= \text{vec} \left\{ -w_{j,n}^{(t)} \cdot \nabla_{p_{j,n}} \left[ \ln p(p_{j,n}^{(t)}) + \ln p(\mathbf{r} | p_{j,n}^{(t)}, \boldsymbol{\theta}_{\sim j}^{(b)}) \right] \right\}_{n=1}^{N_p} \end{aligned} \quad (27)$$

$$\begin{aligned} \nabla_{\mathbf{w}_j} g_j^{(t,b)} &= \nabla_{\mathbf{w}_j} g_j \left( \mathbf{p}_j^{(t)}, \mathbf{w}_j; \boldsymbol{\theta}_{\sim j}^{(b)} \right) \Big|_{\mathbf{w}_j = \mathbf{w}_j^{(t)}} \\ &= \text{vec} \left[ \ln w_{j,n}^{(t)} + 1 - \ln p(p_{j,n}^{(t)}) - \ln p(\mathbf{r} | p_{j,n}^{(t)}, \boldsymbol{\theta}_{\sim j}^{(b)}) \right]_{n=1}^{N_p}. \end{aligned} \quad (28)$$

$\left\{ \boldsymbol{\theta}^{(b)} = [\boldsymbol{\theta}_1^{(b)}, \boldsymbol{\theta}_2^{(b)}, \dots, \boldsymbol{\theta}_J^{(b)}]^T, b = 1, \dots, B \right\}$  is a mini-batch of  $B$  samples generated by the distribution  $\prod_{j=1}^J q(\boldsymbol{\theta}_j; \mathbf{p}_j^{(t)}, \mathbf{w}_j^{(t)})$ , and  $\mathbf{w}^{(b)}$  is the corresponding particle weights for the samples  $\boldsymbol{\theta}^{(b)}$ .  $\rho^{(t)}$  is another decreasing step size that will be discussed below and we set  $\mathbf{f}_{p_j}^{(-1)} = 0, \mathbf{f}_{w_j}^{(-1)} = 0$ . It is worth mentioning that both gradients and iterates (optimization variables) are averaged over iteration. As such, under some technical conditions, almost sure convergence to stationary points can be established.

To ensure the convergence of the algorithm, the step sizes  $\rho^{(t)}$  and  $\gamma^{(t)}$  must satisfy the following step-size rules: 1)  $\rho^{(t)} \rightarrow 0, \sum_t \rho^{(t)} = \infty, \sum_t (\rho^{(t)})^2 < \infty$ ; 2)  $\lim_{t \rightarrow \infty} \gamma^{(t)}/\rho^{(t)} = 0$ . A typical choice of  $\rho^{(t)}, \gamma^{(t)}$  is  $\rho^{(t)} = \mathcal{O}(t^{-\kappa_1}), \gamma^{(t)} = \mathcal{O}(t^{-\kappa_2})$ , where  $0.5 < \kappa_1 < \kappa_2 \leq 1$ . Such form of step sizes have been widely considered in stochastic optimization [13]. The proposed PSPVBI is guaranteed to converge to stationary points of the Problem  $\mathcal{P}_2$ , as will be proved in Section V. After the convergence, the corresponding discrete distribution of each variable  $q(\boldsymbol{\theta}_j)$  composed of particles will approximate the marginal posteriori distribution. As a result, we can take the particle position with the highest probability or the weighted sum of the particles as the final estimate, which are the approximate MAP estimate and MMSE estimate, respectively.

### C. Summary of the PSPVBI Algorithm

The overall PSPVBI algorithm is summarized in Algorithm 1, with its improvements mainly in three aspects. 1) **Flexibility**: Unlike other restricted parametric variational inference algorithms, PSPVBI approximates the posteriori in a non-parametric form (i.e., discrete particles). Higher flexibility in density space makes PSPVBI less prone to getting trapped in local optima, thereby leading to favorable convergence results. Additionally, the update of particle positions provides the algorithm with greater degrees of freedom, enabling it to further enhance performance, accelerate convergence, and reduce the number of particles required. 2) **Efficiency**: To avoid the exponential complexity of multiple integrals in high-dimensional VBI, we apply the PSSCA approach in [12], [13] to improve the sampling efficiency using the average-over-iteration technique. This trick of mini-batch sampling and smoothed recursion avoids scanning over the whole probability space in each update. Given the aforementioned flexibility and efficiency of PSPVBI, we are more likely to obtain accurate global posteriori estimates for high-dimensional, non-convex parameter estimation problems. 3) **Generality**: We extend the SPVBI in [14] from multi-band sensing to more general parameter estimation scenes, and from alternating optimization to parallel optimization to facilitate deep unfolding and convergence acceleration.

As an extension of existing SSCA in [12], with the update of particles in each iteration, the distribution of random states is no longer constant, but changes dynamically, i.e., is control dependent. Nevertheless, under certain technical conditions, convergence can still be guaranteed by constructing a series of parallel sub-surrogate functions. Please refer to Section V-A for the proof.

---

**Algorithm 1** Parallel Stochastic Particle VBI Algorithm
 

---

**Input:** Measurement data, prior  $p(\hat{\theta})$ ,  $\{\rho^{(t)}, \gamma^{(t)}\}$ .

**Initialization:**  $\{p_{j,n}^{(0)} \sim p(\hat{\theta}_j), w_{j,n}^{(0)} = \frac{1}{N_p}\}_{n=1}^{N_p}, \forall j$ .

**While not converge do** ( $t \rightarrow \infty$ )

**Parallel execution for all  $J$  variables:**

    Generate a mini-batch of realization based on the  $\{p_{j,n}^{(t)}, w_{j,n}^{(t)}\}_{n=1}^{N_p}, \forall j$ ;

    Update  $\mathbf{f}_{p_j}^{(t)}$  and  $\mathbf{f}_{w_j}^{(t)}, \forall j$ ;

    Solving surrogate optimization problems;

    Update the particle position and weight of variable  $\theta_j, \forall j$ ;

**end**

**Output:** Find the position  $p_j^*, j = 1, 2, \dots, J$  of the particle with the maximum weight  $w_j^{(max)}$ . (i.e. MAP estimation)

---

#### IV. PROPOSED DEEP-UNFOLDING NETWORK

As a model-driven approach, the PSPVBI algorithm can leverage domain knowledge relevant to the problem, such as signal models and prior information, providing certain performance guarantees. However, it faces challenges during the iterative process, including difficulties in hyperparameter tuning and slow convergence. In contrast, general deep neural networks (DNN) have the capability to automatically learn network parameters through training, exhibiting powerful fitting capabilities [27]. However, they suffer from limited interpretability and generalization abilities. To combine the strengths of both approaches, deep unfolding (DU) techniques in machine learning have been recently introduced [15], [16].

DU networks combine the expressive power of conventional DNNs with the internal structure of model-based methods, while allowing for inference to be performed within a fixed number of layers that can be optimized for best performance. Specifically, DU networks unfold model-driven algorithms with a fixed number of iterations  $T$ , into a layer-wise structure analogous to a neural network with trainable parameters. These parameters are then learned using deep learning (DL) techniques (e.g. suitable loss functions, stochastic gradient descent, and backpropagation). The resulting unfolded algorithm requires fewer iterations and yields optimized network parameters, exhibiting significant advantages. The module design corresponding to Learnable PSPVBI (LPSPVBI) is shown below.

##### A. Module design

The overall network structure is illustrated in Fig. 3, consisting of  $T$  layers cascaded together. Each layer corresponds to one iteration of the original algorithm, including a complete

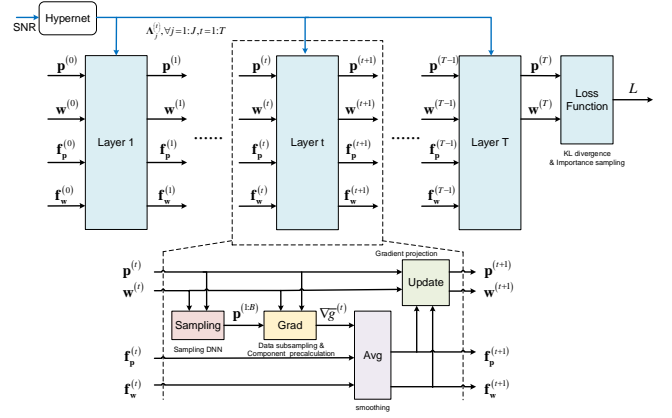


Fig. 3. The architecture of the deep-unfolding framework.

update process of variational distributions for all  $J$  variables. Each layer has the same structure but different trainable parameters<sup>1</sup>  $\Lambda_j^{(t)} = [\Gamma_{w_j}^{(t)}, \Gamma_{p_j}^{(t)}]^T, \forall j = 1 : J, t = 1 : T$ . Particle positions  $\mathbf{p}$ , and weights  $\mathbf{w}$ , and gradients for updating positions and weights  $\mathbf{f}_p, \mathbf{f}_w$  are passed from one layer to another, with each of them being an  $(J \cdot N_p)$ -dimensional vector.

Within each layer, there are four specific modules: 1) sampling module, 2) gradient calculation module, 3) gradient smoothing module, and 4) particle update module. Each module will be introduced in detail below.

1) *Sampling module:* When approximating the gradient in (25) and (26), it is necessary to randomly sample in the state space according to the current discrete variational distributions. This sampling operation should be differentiable due to the backpropagation required by the DU network. A common approach is to use the Gumbel-Softmax method [28], which replaces random nodes with deterministic nodes plus random noise. To some extent, this approximation can mimic random sampling. However, this method introduces significant randomness when generating forward samples and computing backward gradients, resulting in a large variance and making it difficult for the network to converge. Even worse, the logarithmic operator in gradient computation will exacerbate this issue, as the inputs to the logarithmic function are probabilities ranging from 0 to 1. Therefore, it is necessary to generate a sufficient number of samples to ensure that the sampled statistical distribution approximates the probability distribution, resulting in increased computational overhead for each layer.

Since the function mapping that generates a specific number of samples based on the discrete distribution is deterministic, we consider using a simple pre-trained lightweight DNN

<sup>1</sup>The smoothing effect of  $\rho^{(t)}$  on gradients  $\mathbf{f}_{p_j/w_j}^{(t)}$  can be partially achieved by tuning  $\Gamma_{p_j/w_j}^{(t)}$  as a multiplier of  $\mathbf{f}_{p_j/w_j}^{(t)}$  in (18), (19), and since  $\Gamma_{p_j/w_j}^{(t)}$  can directly determine  $\bar{\mathbf{p}}_j^{(t)}/\bar{\mathbf{w}}_j^{(t)}$ , the smoothing effect of  $\gamma^{(t)}$  on variables can also be partially achieved by tuning  $\Gamma_{p_j/w_j}^{(t)}$ . For the purpose of reducing the hyperparameter search space, other step sizes like  $\{\rho^{(t)}, \gamma^{(t)}\}$  are not set as trainable parameters, but are fixed to a set of good empirical values.

network as shown in Fig. 4 to approximate this mapping. The input of DNN is a discrete distribution  $q(\theta_j)$ , consisting of particle positions and particle weights  $\{p_{j,n}^{(t)}, w_{j,n}^{(t)}\}_{n=1}^{N_p}$ , and the output is  $B$  proportional sample values. For example, set  $B = 10$ , if input  $\left\{ \left( p_{j,1}^{(t)}, 0.2 \right), \left( p_{j,2}^{(t)}, 0.3 \right), \left( p_{j,3}^{(t)}, 0.5 \right) \right\}$ ,

the output is  $\left\{ \underbrace{p_{j,1}^{(t)} \dots p_{j,2}^{(t)}}_2, \underbrace{p_{j,2}^{(t)} \dots p_{j,3}^{(t)}}_3, \underbrace{p_{j,3}^{(t)} \dots}_5 \right\}$ . Then, the sampled

values of different variables are shuffled to calculate the gradient. As we all know, DNNs are capable of backpropagation, which satisfies the requirements for subsequent hyperparameter training. Additionally, proportional mapping can effectively indicate the current probability distribution without the need for a large number of random samples.

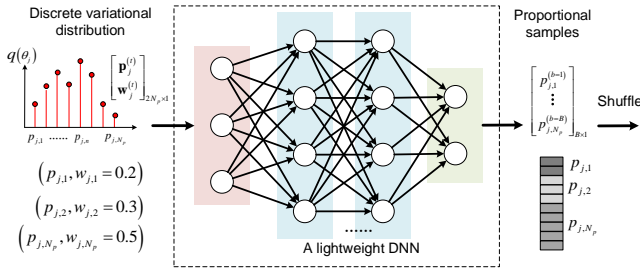


Fig. 4. Illustration of the sampling network.

2) *Gradient calculation module*: Based on (27), (28) and samples  $\theta_j^{(b)}, \forall j, b$ , we can obtain the average gradients of position and weight under several realizations

$$\nabla_{\mathbf{p}_j} \bar{g}^{(t)} = \frac{1}{B} \sum_{b=1}^B \nabla_{\mathbf{p}_j} g_j^{(t,b)}, \quad (29)$$

$$\nabla_{\mathbf{w}_j} \bar{g}^{(t)} = \frac{1}{B} \sum_{b=1}^B \nabla_{\mathbf{w}_j} g_j^{(t,b)}. \quad (30)$$

The major computation bottleneck in (27), (28) lies on calculating  $\ln p(\mathbf{r} | \theta_{\sim j}^{(b)}, p_{j,n}^{(t)})$  and  $\nabla_{p_{j,n}} \ln p(\mathbf{r} | \theta_{\sim j}^{(b)}, p_{j,n}^{(t)})$ . Considering that most variables remain fixed as  $\theta_{\sim j}^{(b)}$  for different particles  $n = 1, \dots, N_p$ , it is possible to precompute certain components and store them for later use during traversal. Furthermore, for high-dimensional  $\mathbf{r} = [r_1, r_2, \dots, r_N]^T$ , we can approximate the likelihood function  $\ln p(\mathbf{r} | \theta)$  with subsampled minibatches  $\Omega \subset \{1, \dots, N\}$  of the data [7]

$$\ln p(\mathbf{r} | \theta) \approx \frac{N}{|\Omega|} \sum_{n \in \Omega} \ln p(\mathbf{r}_n | \theta). \quad (31)$$

As a result, a significant amount of redundant and computationally expensive calculations can be avoided, making the computational cost affordable even in big data settings.

3) *Gradient smoothing module*: The gradient smoothing module is employed to adjust the weighting between historical gradients and the current gradients as shown in (25) and (26). As the iterations advance, the smoothed gradient effectively approximates the true gradient, even when only a small number of samples are used for gradient averaging.

4) *Particle update module*: For updating particle positions,

$$\mathbf{p}_j^{(t+1)} = (1 - \gamma^{(t)}) \mathbf{p}_j^{(t)} + \gamma^{(t)} \text{Proj}_{\Delta p} \left( \mathbf{p}_j^{(t)} - \Gamma_{p_j}^{(t)} \mathbf{f}_{p_j}^{(t)} \right). \quad (32)$$

Due to the quadratic surrogate function and box constraints in  $\mathcal{P}_2$ , the projection operation  $\text{Proj}_{\Delta p}(\cdot)$  can be expressed as a simple piecewise function

$$\text{Proj}_{\Delta p}(x) = \begin{cases} a & x \in (-\infty, a) \\ x & x \in [a, b] \\ b & x \in (b, +\infty) \end{cases}, \quad (33)$$

where  $a = \hat{\theta}_j - \Delta \hat{\theta}_j / 2$ ,  $b = \hat{\theta}_j + \Delta \hat{\theta}_j / 2$ . Its derivative is

$$\nabla \text{Proj}_{\Delta p}(x) = \begin{cases} 1 & x \in [a, b] \\ 0 & \text{otherwise} \end{cases}.$$

For updating particle weights,

$$\mathbf{w}_j^{(t+1)} = (1 - \gamma^{(t)}) \mathbf{w}_j^{(t)} + \gamma^{(t)} \text{Proj}_{\Delta w} \left( \mathbf{w}_j^{(t)} - \Gamma_{w_j}^{(t)} \mathbf{f}_{w_j}^{(t)} \right). \quad (34)$$

Since the constraint conditions of the subproblem are coupled simplex constraints in  $\mathcal{P}_2$ , the projection operation can be iteratively accomplished using the intuitive alternating projection method. It should be noted that the alternating projection method is not the most efficient method for solving this problem [29]. However, considering that the entire projection process needs to support gradient backpropagation, it was suitable to use this approach in the DU network. We define sets  $\mathbb{C}_1 = \{ \mathbf{w}_j \in \mathbb{R}^{N_p} : \mathbf{w}_j \cdot \mathbf{1}_{N_p}^T = 1 \}$  and  $\mathbb{C}_2 = \{ \mathbf{w}_j \in \mathbb{R}^{N_p} : w_{j,n} \geq \epsilon, n = 1, \dots, N_p \}$ , where  $\mathbf{1}_{N_p}$  is a  $N_p$ -dimensional vector of ones. By alternately projecting onto set  $\mathbb{C}_1$  and set  $\mathbb{C}_2$ , after a few steps, we can obtain the result projected onto the simplex [30]. Details of the alternating projection are provided below.

---

#### Algorithm 2 Alternating Projection Method.

---

**Input:**  $\mathbf{w}_j$ . (Initialization:  $\mathbf{y}_r = \mathbf{y}_{r+1} = \mathbf{w}_j, error = +\infty, \epsilon \rightarrow 0$ )

**While** ( $error > 10^{-6}$ )

$$\mathbf{y}_{r+1} = \max \left\{ \left[ \mathbf{y}_r - \frac{1}{N_p} \left( \mathbf{y}_r \cdot \mathbf{1}_{N_p}^T - 1 \right) \mathbf{1}_{N_p} \right], \epsilon \cdot \mathbf{1}_{N_p} \right\}$$

$$error = \|\mathbf{y}_{r+1} - \mathbf{y}_r\|_2;$$

$$\mathbf{y}_r = \mathbf{y}_{r+1};$$

**end**

**Output:**  $\mathbf{y}_r$ .

---

Hence, its derivative is  $\nabla \text{Proj}_{\Delta w}(\mathbf{w}) = \left[ \left( \mathbf{I}_{N_p \times N_p} - \frac{1}{N_p} \text{diag}(\mathbf{I}(\mathbf{w})) \right) \right]^{iter}$ ,  $I(x) = \begin{cases} 1 & x \geq \epsilon \\ 0 & x < \epsilon \end{cases}$ , where  $iter$  represents the number of iterations for alternating projection,  $\mathbf{I}_{N_p \times N_p}$  is a  $N_p \times N_p$ -dimensional identity matrix.

5) *Hypernetwork design*: Despite the LPSPVBI network achieving considerable estimation performance with faster convergence after training, there is still performance degradation due to a mismatch between the training and testing environments. This occurs because the variables learned under specific conditions are not suitable for different scenarios. For example, if the LPSPVBI is trained using data generated with SNR = 15dB, its performance will decline when tested



with SNR = 10dB. To address this issue, we introduce the Hypernetwork [20] into the LPSPVBI framework.

A hypernetwork, short for 'hyperparameter network', is a type of neural network architecture used in deep learning. It is designed to dynamically generate or learn the parameters of another neural network (i.e. target network) based on input data. Due to the high correlation between the training parameters and the SNR (or noise precision), we use the SNR and training parameters  $\mathbf{A} \in \mathbb{R}^{2J \cdot T \times 1}$  as the inputs and outputs of the hypernetwork. Subsequently, a classical three-layer fully connected hypernetwork is adopted to learn such a mapping in order to enhance the generalization capability of LPSPVBI in different noise environments, which can be written as

$$\mathbf{A} = \mathbf{W}_3 \cdot \text{ReLU}(\mathbf{W}_2 \cdot \text{ReLU}(\mathbf{W}_1 \cdot \text{SNR} + \mathbf{b}_1) + \mathbf{b}_2) + \mathbf{b}_3, \quad (35)$$

where  $\mathbf{W}_{1,2,3}$  and  $\mathbf{b}_{1,2,3}$  are the parameters to be trained for the Hypernetwork.

In addition, for the parameter estimation scenario, the number of variables  $J$  is usually not constant, such as the number of paths and the targets. To make the unfolded algorithm adaptive to different  $J$ , we can train our network with a larger  $J_0$  in advance, so that it can be straightforwardly transferred to the scenarios with  $J \leq J_0$ . In the inference stage, we only need to set  $\left\{ \mathbf{p}_j^{(0)}, \mathbf{w}_j^{(0)}, \mathbf{f}_{p,j}^{(0)}, \mathbf{f}_{w,j}^{(0)} \right\}_{j=J+1}^{J_0} = 0$  when  $J < J_0$ .

## B. Training Details

1) *Loss function*: As the objective function of the PSPVBI algorithm in  $\mathcal{P}_2$ , the KL divergence is defined as the loss function of DU, which measures the distance between the variational distribution  $q(\boldsymbol{\theta})$  after  $T$  iterations and the true posteriori distribution  $p(\boldsymbol{\theta}|\mathbf{r})$ :

$$\text{Loss} \triangleq \int q(\boldsymbol{\theta}; \mathbf{p}^{(T)}, \mathbf{w}^{(T)}) \ln \frac{q(\boldsymbol{\theta}; \mathbf{p}^{(T)}, \mathbf{w}^{(T)})}{p(\mathbf{r}|\boldsymbol{\theta})p(\boldsymbol{\theta})} d\boldsymbol{\theta}. \quad (36)$$

Similar to the approach of approximating gradients through sampling, we can adopt Monte Carlo sampling to approximate the above multiple integral. To improve the accuracy of the loss function, it is advisable to increase the number of samples used, for example,  $B = 500$ .

2) *Back propagation*: According to the loss function in (36), we can first obtain the gradients with respect to the final layer's particle positions and weights:

$$\begin{aligned} \frac{\partial \text{Loss}}{\partial \mathbf{p}_j^{(T)}} &\triangleq \mathbb{E}_{q(\boldsymbol{\theta}; \mathbf{p}^{(T)}, \mathbf{w}^{(T)})} \left[ \frac{\partial g^{(T)}}{\partial \mathbf{p}_j^{(T)}} \right] \\ &\approx \frac{1}{B_{\text{grad}}} \sum_{b=1}^{B_{\text{grad}}} \nabla_{\mathbf{p}_j} g_j^{(T)} \left( \mathbf{p}_j^{(T)}; \mathbf{w}_j^{(T)}, \boldsymbol{\theta}_{\sim j}^{(b)} \right), \end{aligned} \quad (37)$$

$$\begin{aligned} \frac{\partial \text{Loss}}{\partial \mathbf{w}_j^{(T)}} &\triangleq \mathbb{E}_{q(\boldsymbol{\theta}; \mathbf{p}^{(T)}, \mathbf{w}^{(T)})} \left[ \frac{\partial g^{(T)}}{\partial \mathbf{w}_j^{(T)}} \right] \\ &\approx \frac{1}{B_{\text{grad}}} \sum_{b=1}^{B_{\text{grad}}} \nabla_{\mathbf{w}_j} g_j^{(T)} \left( \mathbf{w}_j^{(T)}; \mathbf{p}_j^{(T)}, \boldsymbol{\theta}_{\sim j}^{(b)} \right). \end{aligned} \quad (38)$$

After obtaining the final layer's gradients, we can perform gradient backpropagation using the chain rule of differentiation to get other layers' gradients  $\frac{\partial \text{Loss}}{\partial \mathbf{p}_j^{(t)}}, \frac{\partial \text{Loss}}{\partial \mathbf{w}_j^{(t)}}, \frac{\partial \text{Loss}}{\partial \mathbf{f}_{p,j}^{(t)}}, \frac{\partial \text{Loss}}{\partial \mathbf{f}_{w,j}^{(t)}}, \forall t = (T-1), \dots, 2, 1$ . Then, we can further obtain the gradients of the loss function with respect to the hyperparameters  $\mathbf{A}_j^{(t)}$  of each layer

$$\frac{\partial \text{Loss}}{\partial \mathbf{A}_j^{(t)}} = \frac{\partial \text{Loss}}{\partial \mathbf{p}_j^{(t+1)}} \cdot \frac{\partial \mathbf{p}_j^{(t+1)}}{\partial \mathbf{A}_j^{(t)}} + \frac{\partial \text{Loss}}{\partial \mathbf{w}_j^{(t+1)}} \cdot \frac{\partial \mathbf{w}_j^{(t+1)}}{\partial \mathbf{A}_j^{(t)}}, \quad (39)$$

where  $\frac{\partial \mathbf{p}_j^{(t+1)}}{\partial \Gamma_{p_j}^{(t)}} = \gamma^{(t)} \left( -\mathbf{f}_{w_j}^{(t)} \right) \nabla \text{Proj}_{\Delta w}$ ,  $\frac{\partial \mathbf{p}_j^{(t+1)}}{\partial \Gamma_{w_j}^{(t)}} = 0$ ,  $\frac{\partial \mathbf{w}_j^{(t+1)}}{\partial \Gamma_{p_j}^{(t)}} = 0$ ,  $\frac{\partial \mathbf{w}_j^{(t+1)}}{\partial \Gamma_{w_j}^{(t)}} = \gamma^{(t)} \left( -\mathbf{f}_{p_j}^{(t)} \right) \nabla \text{Proj}_{\Delta p}$ . Finally, we use the gradients as a loss function of the Hypernetwork described in IV-A5 to train the parameters  $\mathbf{W}_{1,2,3}$  and  $\mathbf{b}_{1,2,3}$ .

By conducting practical tests or simulating different wireless environments (i.e. SNR, delay path, etc.), we can obtain a large amount of training data. Additionally, training techniques from machine learning, such as mini-batch averaging, stochastic gradient descent (SGD), Adam optimization [31], and others, can be applied to train the hyperparameters of the DU network. The detailed training procedures of the LPSPVBI are presented in Algorithm 3.

---

**Algorithm 3** The training procedures of PSPVBI-Inspired Deep-Unfolding Network.

---

Given the training set. Set the number of layers  $T$ , the batch size  $N_{\text{batch}}$ , the tolerance of accuracy, the maximum iteration number  $I_{\text{max}}$ , and the current iteration index of the training stage  $\text{iter} = 0$ .

### Repeat

**1. Forward propagation**: Select a group of samples from the training set and initialize  $\left\{ \mathbf{p}^{(0)}, \mathbf{w}^{(0)}, \mathbf{f}_p^{(0)}, \mathbf{f}_w^{(0)} \right\}$ . Compute  $\left\{ \mathbf{p}^{(t)}, \mathbf{w}^{(t)}, \mathbf{f}_p^{(t)}, \mathbf{f}_w^{(t)} \right\}, \forall t = 1, \dots, T$  based on (18)-(21).

**2.** Then plug  $\left\{ \mathbf{p}^{(T)}, \mathbf{w}^{(T)} \right\}$  into the loss function and obtain its value.

**3. Backward propagation**: Firstly, compute the gradients with respect to variables  $\left\{ \mathbf{p}^{(T)}, \mathbf{w}^{(T)} \right\}$  in the last layer based on (37)-(38). Secondly, compute the gradients of  $\left\{ \mathbf{p}^{(t)}, \mathbf{w}^{(t)}, \mathbf{f}_p^{(t)}, \mathbf{f}_w^{(t)} \right\}, \forall t = (T-1), \dots, 2, 1$  according to the chain rule. Finally, compute the gradients of trainable parameters and based on (39).

**4. Update Hypernetwork parameters**: Repeat steps 1 – 3 for  $N_{\text{batch}}$  times and compute the average gradients of trainable parameters in a batch. Then, apply mini-batch SGD to update the Hypernetwork parameters.

**5.**  $\text{iter} = \text{iter} + 1$ .

**Until** the loss function in the validation set converges or  $\text{iter} \geq I_{\text{max}}$ .

---

## V. CONVERGENCE ANALYSIS

In this section, we will present the convergence analysis of the PSPVBI algorithm and the deep-unfolded LPSPVBI algorithm.

### A. Convergence analysis of PSPVBI

In this subsection, we show that the proposed PSSCA-based PSPVBI algorithm can be guaranteed to converge to a stationary solution of  $\mathcal{P}_2$ .

Firstly, we point out that the gradient projection operation (18), (19) in PSPVBI can be viewed as solving a constrained quadratic surrogate subproblem, as illustrated in Fig. 5. Moreover, the convex quadratic surrogate functions  $\bar{f}_{p_j}^{(t)}(\mathbf{p}_j)$  and  $\bar{f}_{w_j}^{(t)}(\mathbf{w}_j)$  (i.e. (16), (17)) in this context possess the property of asymptotic consistency, which is given in the key lemma below.

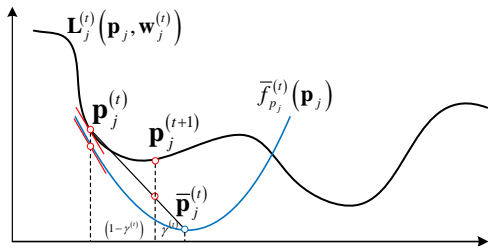


Fig. 5. An illustration of stochastic successive convex approximation.

#### Lemma 3 (Asymptotic consistency of surrogate functions).

For each iteration  $t = 1, 2, \dots$  and each  $\mathbf{p}_j, \mathbf{w}_j, j = 1, 2, \dots, J$ , consider a subsequence  $\{\mathbf{p}^{(t_i)}, \mathbf{w}^{(t_i)}\}_{i=1}^{\infty}$  converging to a limit point  $\mathbf{p}^*, \mathbf{w}^*$ . There exist uniformly differentiable functions  $\hat{f}_{p_j}(\mathbf{p}_j)$  and  $\hat{f}_{w_j}(\mathbf{w}_j)$  such that

$$\lim_{i \rightarrow \infty} \bar{f}_{p_j}^{(t_i)}(\mathbf{p}_j) = \hat{f}_{p_j}(\mathbf{p}_j), \forall \mathbf{p}_j, \quad (40)$$

$$\lim_{i \rightarrow \infty} \bar{f}_{w_j}^{(t_i)}(\mathbf{w}_j) = \hat{f}_{w_j}(\mathbf{w}_j), \forall \mathbf{w}_j. \quad (41)$$

Moreover, we have

$$\left\| \nabla_{\mathbf{p}_j} \hat{f}_{p_j}(\mathbf{p}_j^*) - \nabla_{\mathbf{p}_j} L(\mathbf{p}^*, \mathbf{w}^*) \right\| = 0, \quad (42)$$

$$\left\| \nabla_{\mathbf{w}_j} \hat{f}_{w_j}(\mathbf{w}_j^*) - \nabla_{\mathbf{w}_j} L(\mathbf{p}^*, \mathbf{w}^*) \right\| = 0. \quad (43)$$

Please refer to Appendix A for the proof. With the Lemma 3, we are ready to prove the following main convergence result.

**Theorem 4 (Convergence of PSPVBI).** Starting from a feasible initial point  $\{\mathbf{p}^{(0)}, \mathbf{w}^{(0)}\}$ , let  $\{\mathbf{p}^{(t)}, \mathbf{w}^{(t)}\}_{t=1}^{\infty}$  denote the iterates generated by Algorithm 1. Then every limiting point  $\mathbf{p}^*, \mathbf{w}^*$  of  $\{\mathbf{p}^{(t)}, \mathbf{w}^{(t)}\}_{t=1}^{\infty}$  is a stationary point of optimization problem  $\mathcal{P}_2$  almost surely.

The proof is similar to that of ([32], Theorem 3) and is omitted for conciseness.

### B. Convergence analysis of deep-unfolded LPSPVBI

For deep-unfolding networks, if the iterated algorithm being unfolded is convergent and the network structure is appropriate, it can typically achieve convergence after effective training. However, it is difficult to provide a rigorous proof of convergence for the deep-unfolded LPSPVBI. Therefore, in

this section, we will intuitively explain the reason why such an approach works.

Firstly, let us investigate the connection between the deep-unfolded LPSPVBI and the PSSCA-based PSPVBI algorithm. It is obvious that the LPSPVBI has a similar structure with the parallel SSCA. However, the LPSPVBI introduces learnable parameters to accelerate convergence. Thus, LPSPVBI inherits almost all of PSPVBI's convergence properties, without altering the original algorithm's working mechanism.

Secondly, proposed algorithm essentially searches for a particle-based variational distribution in the density space that best fits the true posteriori, based on a gradient descent strategy. As pointed out in [33], any gradient descent-type algorithm selects a direction  $\mathbf{d}^{(i)}$ , then searches along this direction with an appropriate step size  $\eta^{(i)}$  to obtain a new iteration that achieves a smaller distance to the optimal solution  $\mathbf{s}^*$ . Suppose after  $I$  iterations, we can find the optimal solution, i.e.,

$$\mathbf{s}^* = \hat{\mathbf{s}}^{(0)} + \eta^{(0)} \mathbf{d}^{(0)} + \dots + \eta^{(I-1)} \mathbf{d}^{(I-1)}. \quad (44)$$

The above process can be seen as finding a set of vectors (directions) and corresponding weights (step sizes) whose weighted linear combination equals  $\mathbf{s}^* - \hat{\mathbf{s}}^{(0)}$ . In the PSPVBI algorithm, the step sizes are fixed, requiring a larger number of iterations to approximate the optimal solution. However, the LPSPVBI algorithm tries to find a more optimal set of stepsizes, such that the number of iterations can be restricted to the depth of the network. In addition, due to the existence of non-linear operator (i.e. projection) and smoothing operator, the step sizes can also affect the descent direction.

Therefore, the proposed LPSPVBI algorithm can achieve convergence in a given number of layers with a high probability.

## VI. APPLICATIONS

As mentioned earlier, deriving Bayesian inference-based algorithms one by one for each model is a tedious task [8]. However, our proposed LPSPVBI algorithm framework effectively addresses this issue. Based on (27) and (28), all that is required is to provide prior information, model-dependent likelihood function and training data, to accomplish variational approximation of the posteriori distribution and parameter fine-tuning. Its strong generality allows practitioners to rapidly design, apply, and modify their data models without the need to laboriously derive and debug every time.

We shall apply the proposed LPSPVBI to solve the two application problems in Section II.

### A. Example 1 (Wireless cooperative localization)

Consider the wireless cooperative localization problem in Example 1. The logarithmic likelihood function and logarithmic prior distribution for this example are

$$\ln p(\mathbf{s}_i) = \frac{1}{2} \ln \frac{|\mathbf{U}_i|}{2\pi} + \left[ -\frac{1}{2} (\mathbf{s}_i - \boldsymbol{\mu}_i)^T \mathbf{U}_i (\mathbf{s}_i - \boldsymbol{\mu}_i) \right], \quad (45)$$

$$\ln p(\mathbf{z} | \mathbf{s}_0, \mathbf{c}) = \frac{N_R}{2} \ln \frac{|U_{ni}|}{2\pi} + \sum_{i=1}^{N_R} \left[ -\frac{U_{ni}}{2} (\mathbf{z}_i - h(\mathbf{s}_i, \mathbf{s}_0))^2 \right]. \quad (46)$$

Additionally, the first derivatives are

$$\frac{\partial \ln p(\mathbf{s}_i)}{\partial \mathbf{s}_i} = -\mathbf{U}_i(\mathbf{s}_i - \boldsymbol{\mu}_i), \forall i = 0, 1, \dots, N_R, \quad (47)$$

$$\frac{\partial \ln p(\mathbf{z}|\mathbf{s}_0, \mathbf{c})}{\partial \mathbf{s}_0} = \sum_{i=1}^{N_R} \left[ U_{ni}(\mathbf{z}_i - h(\mathbf{s}_i, \mathbf{s}_0)) \frac{10\lambda}{\ln 10} \frac{(\mathbf{s}_i - \mathbf{s}_0)}{\|\mathbf{s}_i - \mathbf{s}_0\|_2^2} \right]. \quad (48)$$

1) *Performance Comparison*: We use a similar simulation configuration as that in [6]. There are  $N_R = 6$  reference nodes and a target node in a RSS-based localization scenario, as shown in Fig. 1. The precision of each node initial location is assumed to be  $\mathbf{U}_i = 1/10\mathbf{I}, \forall i = 0, 1, \dots, N_R$ , where  $\mathbf{I}$  denotes the identity matrix. We assume in all simulations that,  $\lambda = 3$  and  $\phi_{ref} = -5dBm$ . In addition, we assume  $r_s = 50[m]$ ,  $\varepsilon_i = 4/75$ .

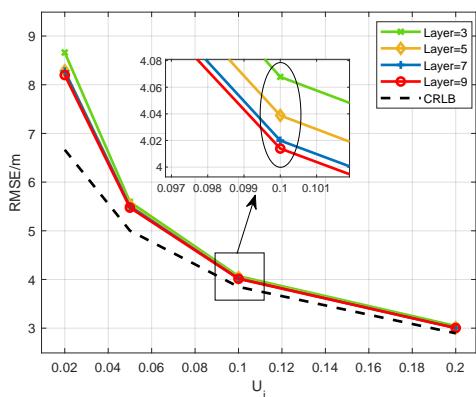


Fig. 6. Localization error of different layers over various priori location precisions for LPSPVBI.

In Fig. 6, We plotted the localization error for different depths under various prior precisions. In general, with more accurate priors, the positioning error becomes smaller, and the gap with the Cramer-Rao Lower Bound (CRLB) also decreases. Furthermore, as we increase the number of network layers from 3 to 9, localization accuracy gradually improves and almost ceases to improve after reaching a certain number of layers, such as 7 layers.

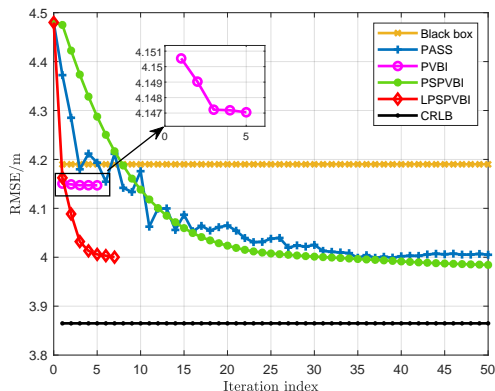


Fig. 7. RSS-based localization errors with different methods.

Then, in Fig. 7, we compare the performance and convergence of the proposed PSPVBI, LPSPVBI, and other

algorithms. **1) Blackbox**: To compare with the dual-driven (i.e. model and data) DU network, we introduce conventional black-box based DNNs as a benchmark. Its input is a vector composed of measurements and prior information about nodes, which sequentially passes through fully connected (FC) layers, batch normalization (BN), and non-linear functions. The DNN's output is the position of the target node. We use leaky ReLU as the activation function and the Adam optimization method. **2) PASS** [6]: As a particle-based stochastic search algorithm, PASS lacks theoretical convergence guarantees and heuristically drives other particles towards the one with the maximum approximate posteriori probability. **3) PVBI** [3]: PVBI did not update particle positions and directly computed the multiple summations without using stochastic approximations. A total of 1000 experiments were repeated to obtain the averaged iteration curves shown as in Fig. 7. It can be seen that the LPSPVBI achieves performance similar to PSPVBI and PASS in very few iterations, demonstrating that DU effectively accelerates the algorithm's convergence.

2) *Computational Complexity*: For PVBI algorithm, its per-iteration complexity order is  $\mathcal{O}(J \cdot (N_p)^4 F_{LH})$ , where  $F_{LH}$  represents the average number of floating point operations (FLOPs) required to compute the dominant logarithmic likelihood value. For PSPVBI algorithm, through mini-batch sampling and minimization of quadratic surrogate objective functions, the per-iteration complexity can be reduced to  $\mathcal{O}(2J \cdot (N_p B F_{grad} + N_p^3))$ , where  $F_{grad}$  and  $N_p^3$  represent the complexity of computing a gradient and projection, respectively. For LPSPVBI algorithm, the main complexity lies in the gradient calculation module, and the complexity of other modules can be neglected. For PASS algorithm,  $N_R$  represents the number of reference nodes, while  $N_S$ ,  $N_D$  and  $N_M$  represent the counts of search particles, detection particles, and proposal particles respectively.  $F_{belief}$  denotes the number of FLOPs required to compute a single belief. For black-box based DNN,  $L_{0\sim 3}$  are the sizes of each layer in DNN.  $T_{1\sim 4}$  are the typical number of iterations of each algorithm.

In Table I, we summarize the complexity order of different algorithms, and numerically compare them under a typical setting as follows:  $T_1 = 3$ ,  $J = 2$ ,  $N_R = 6$ ,  $N_p = 10$ ,  $F_{LH} = 60$ ;  $T_2 = 35$ ,  $N_S = 20$ ,  $N_D = 6$ ,  $N_M = 5$ ,  $F_{belief} = 10$ ;  $T_3 = 25$ ,  $B = 20$ ,  $F_{grad} = 36$ ;  $L_1 = 22$ ,  $L_2 = L_3 = 512$ ,  $L_4 = 2$ ;  $T_4 = 7$ . It can be seen that, compared to other algorithms, LPSPVBI greatly reduces the computational complexity while maintaining performance.

TABLE I  
COMPARISON OF THE COMPLEXITY ORDER FOR DIFFERENT ALGORITHMS IN EXAMPLE 1

Algorithms	Complexity order	Typical values
PVBI	$\mathcal{O}(T_1 J \cdot (N_p)^4 F_{LH})$	$36 \times 10^5$
PASS	$\mathcal{O}(T_2 N_R N_S N_D N_M F_{belief})$	$12.6 \times 10^5$
PSPVBI	$\mathcal{O}(T_3 2J \cdot (N_p B F_{grad} + N_p^3))$	$8.20 \times 10^5$
Black-box	$\mathcal{O}(\sum_{i=0}^2 L_{i+1} L_i)$	$2.74 \times 10^5$
LPSPVBI	$\mathcal{O}(T_4 2J \cdot (N_p B F_{grad} + N_p^3))$	$2.30 \times 10^5$

### B. Example 2 (Multiband WiFi sensing)

Consider a multi-band WiFi sensing system in Example 2, where WiFi signals from multiple non-contiguous frequency bands are utilized for ranging purposes. In this scenario, explicit expressions of the gradient  $\nabla_{\mathbf{p}_j} g_j^{(t,b)}$  and  $\nabla_{\mathbf{w}_j} g_j^{(t,b)}$  in (27) and (28) are given in the Appendix of [32].

1) *Performance Comparison*:: In the simulations, each variable is equipped with  $N_p = 10$  particles, and the size of mini-batch  $B$  is 10. The received signals come from two non-adjacent frequency bands with a bandwidth of 20MHz. The initial frequency is set to 2.4GHz and 2.46GHz, respectively. The subcarrier spacing is 78.125KHz. There are two scattering paths with delays uniformly generated between 20ns and 200ns. The amplitudes  $\alpha_k$  are 1 and 0.5, and the phases  $\beta_k$  are  $-\pi/4$  and  $\pi/4$ , respectively. In addition, initial phase  $\phi_m$  are uniformly generated within  $[0, 2\pi]$ . The timing synchronization error  $\delta_m$  is generated following a Gaussian distribution  $\mathcal{N}(0, 0.01\text{ns}^2)$ . The step size sequence is set as follows:  $\rho^{(t)} = 5/(5+t)^{0.9}$ ,  $\rho^{(0)} = 1$ ;  $\gamma^{(t)} = 5/(15+t)^1$ ,  $\gamma^{(0)} = 1$ . Unless otherwise specified, the experiment was repeated 400 times.

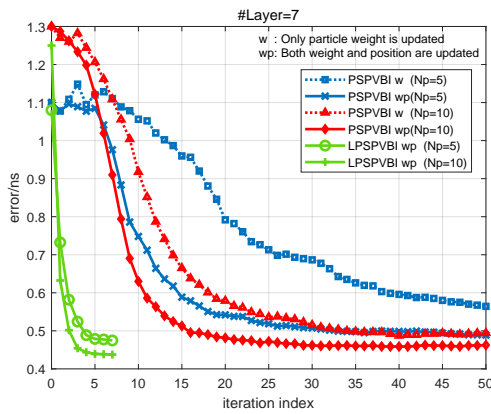


Fig. 8. Iteration error curves with different particle numbers.

In Fig. 8, we plot the convergence curves of different updating modes with different number of particles. As the number of particles decreases from 10 to 5, it can be seen that the convergence speed will slow down when only the weight is updated, but the convergence speed and performance will almost remain the same when the position is also updated. This means that updating the position of particles can effectively increase the degree of freedom of optimization and ensure convergence and performance even with fewer particles.

In Fig. 9, we compare the proposed algorithm with the following baseline algorithms: **1) Weighted Root-MUSIC (WR-MUSIC)** [34]: As an improved subspace-based algorithm, WR-MUSIC can serve as a leading algorithm to provide prior information for the PSPVBI. Please refer to [32] for specific details. **2) Blackbox**: The structure of black-box based DNN is similar to that in Example 1. It can be seen that the performance of all algorithms improves as the signal-to-noise ratio (SNR) increases from 5dB to 20dB. Furthermore, under the adjustment of the Hypernet, the LPSPVBI algorithm can adapt well to varying SNR conditions. At a certain SNR, the

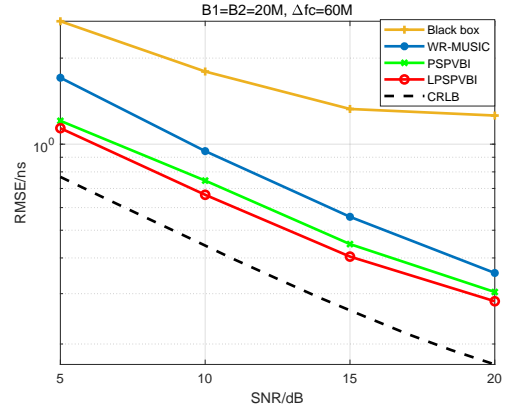


Fig. 9. RMSE of delay estimation with respect to the SNR.

root-mean-square error (RMSE) of LPSPVBI is closer to the CRLB and significantly lower than that of other algorithms, indicating higher time delay estimation accuracy. In addition, compared to Example 1, Example 2 has a higher-dimensional variable space and more local optima, making the superiority of the proposed algorithm more pronounced.

2) *Computational Complexity*:: For WR-MUSIC algorithm, it mainly includes subspace decomposition and polynomial rooting, with the complexity of  $\mathcal{O}(MN_m^3)$  and  $\mathcal{O}(M(2N_m - 1)^3)$ . The complexity analysis of other algorithms is similar to Section VI-A2.

In Table II, we summarize the complexity order of different algorithms, and numerically compare them under a typical setting as follows:  $M = 2$ ,  $N_m = 256$ ;  $L_0 = 1028$ ,  $L_1 = 3072$ ,  $L_2 = 4096$ ,  $L_3 = 2048$ ,  $L_4 = 256$ ,  $L_5 = 2$ ;  $T_1 = 3$ ,  $J = 9$ ,  $N_p = 10$ ,  $F_{LH} = 5000$ ,  $|\Omega| = 64$ ;  $T_2 = 35$ ,  $T_3 = 7$ ,  $B = 10$ ,  $F_{grad} = 4500$ .

TABLE II  
COMPARISON OF THE COMPLEXITY ORDER FOR DIFFERENT ALGORITHMS IN EXAMPLE 2

Algorithms	Complexity order	Typical values
PVBI <sup>2</sup>	$\mathcal{O}(T_1 J \cdot (N_p)^J F_{LH})$	$1.35 \times 10^{14}$
WR-MUSIC	$\mathcal{O}(MN_m^3 + M(2N_m - 2)^3)$	$2.99 \times 10^8$
PSPVBI	$\mathcal{O}(T_2 2J \cdot (N_p B F_{grad} + N_p^3))$	$2.84 \times 10^8$
LPSPVBI	$\mathcal{O}(T_3 2J \cdot (N_p B F_{grad} + N_p^3))$	$5.68 \times 10^7$
Black-box	$\mathcal{O}(\sum_{i=0}^4 L_{i+1} L_i)$	$2.47 \times 10^7$

By comparing the performance and complexity of the algorithms before and after unfolding, we can conclude that deep-unfolding indeed fully unleashes the algorithm's potential.

## VII. CONCLUSIONS

In this paper, we consider a general parameter estimation problem in sensing scenarios. Within the framework of Bayesian estimation, parameter estimation is transformed into a variational optimization problem aimed at approximating the

<sup>2</sup>Due to the large number of variables in this scenario, PVBI algorithm with excessive computational complexity is not applicable. The performance comparison between PVBI and PSPVBI in a simplified scenario can be found in [32].

true posteriori distribution. To address it, we propose a parallel stochastic particle variational Bayesian inference (PSPVBI) algorithm to find a stationary point of this problem. Compared to conventional VBI, particle approximation and particle position update make it more flexible and faster in fitting the posteriori distribution. Furthermore, the introduction of parallel stochastic successive convex approximation (PSSCA) also effectively addresses the pain point of high computational complexity in variational inference. To further reduce complexity, we perform a deep-unfolding for PSPVBI algorithm by constructing a model-driven deep learning network. The derived learnable PSPVBI (LPSPVBI) algorithm can further decrease the number of iterations and single-iteration complexity. Some techniques related to subsampling, gradient computation, and generalization ability used in this approach also contribute to the practical deployment of the algorithm. Finally, we use several important application examples to demonstrate the effectiveness of the proposed algorithm. The low-complexity LPSPVBI algorithm holds the potential to be applied in a broad range of high-dimensional, non-convex parameter estimation scenarios, even with numerous local optima and non-conjugate priors.

## APPENDIX

### A. Proof of Lemma 3

We first introduce the following preliminary result.

**Lemma 5.** *Given problem  $\mathcal{P}_2$ , suppose that the step sizes  $\rho^{(t)}$  and  $\gamma^{(t)}$  are chosen according to step-size rules in III-B. Let  $\{\mathbf{p}^{(t)}, \mathbf{w}^{(t)}\}$  be the sequence generated by Algorithm 1. Then, the following holds*

$$\lim_{t \rightarrow \infty} \left| \mathbf{f}_{p_j}^{(t)} - \nabla_{\mathbf{p}_j} \mathbf{L}(\mathbf{p}^{(t)}, \mathbf{w}^{(t)}) \right| = 0, w.p.1. \quad (49)$$

$$\lim_{t \rightarrow \infty} \left| \mathbf{f}_{w_j}^{(t)} - \nabla_{\mathbf{w}_j} \mathbf{L}(\mathbf{p}^{(t)}, \mathbf{w}^{(t)}) \right| = 0, w.p.1. \quad (50)$$

*Proof:* Lemma 5 is a consequence of ([35], Lemma 1). We only need to verify that all the technical conditions (a)–(e) therein are satisfied. Specifically, Condition (a) of ([35], Lemma 1) is satisfied because domains of particle positions  $\mathbf{p}$  and weights  $\mathbf{w}$  are compact and bounded. Furthermore, the boundedness of  $\mathbf{p}$  and  $\mathbf{w}$  ensures that the logarithmic terms in (27) and (28) do not tend towards infinity. As a result, the instantaneous gradient  $\nabla g_j^{(t)}$  (i.e.  $\nabla_{\mathbf{p}_j/\mathbf{w}_j} g_j^{(t)}$ ) remains bounded, satisfying Condition (b) of ([35], Lemma 1). Conditions (c)–(d) directly derived from the step-size rule 1) in III-B. When the particles of all variables are updated in parallel, the distributions (i.e., positions and weights of particles) are no longer identical over iterations, but change slowly at the rate of order  $\mathcal{O}(\gamma^{(t)})$ , which causes the random state  $\theta$  in the objective function to change constantly. Due to the boundedness of  $\mathbf{p}$  and  $\mathbf{w}$ , all the logarithmic terms in the instantaneous gradient  $\nabla g_j^{(t)}$  are Lipschitz continuous. Therefore,  $\nabla g_j^{(t)}$  is also Lipschitz continuous, and  $\left\| \nabla g_j^{(t+1)} - \nabla g_j^{(t)} \right\| = \mathcal{O}(\gamma^{(t)})$ . Additionally, the expectation operator (i.e. the multiplication and addition operations with  $\mathbf{w}$ ) slows down the change of  $\nabla \mathbf{L}_j^{(t)}$  (i.e.  $\nabla_{\mathbf{p}_j/\mathbf{w}_j} \mathbf{L}^{(t)}$ ),

resulting in  $\left\| \nabla \mathbf{L}_j^{(t+1)} - \nabla \mathbf{L}_j^{(t)} \right\| = \mathcal{O}^2(\gamma^{(t)})$ . Plusing the step-size rule 2) in III-B, Condition (e) of ([35], Lemma 1)  $\left\| \nabla \mathbf{L}_j^{(t+1)} - \nabla \mathbf{L}_j^{(t)} \right\| / \rho^{(t)} \rightarrow 0$  is also satisfied. ■

As can be seen, Lemma 3 requires proof for two parts. Similar to the proof in ([12], Lemma 1), we first establish the existence of the limit of the surrogate function sequence, i.e., (40) and (41).

Since the surrogate functions adopted are convex quadratic functions with box constraints/simplex constraints, it is straightforward to determine that they possess the following properties. For any  $\mathbf{p}_j \in \mathcal{X}_p$  and  $\mathbf{w}_j \in \mathcal{X}_w$ ,  $\bar{f}_{p_j}^{(t)}(\mathbf{p}_j)$  and  $\bar{f}_{w_j}^{(t)}(\mathbf{w}_j)$  are uniformly strongly convex and Lipschitz continuous, and their derivative, second order derivative are uniformly bounded [12], [14]. Due to these properties of the surrogate functions, the families of functions  $\left\{ \bar{f}_{p_j}^{(t_i)}(\mathbf{p}_j) \right\}$  and  $\left\{ \bar{f}_{w_j}^{(t_i)}(\mathbf{w}_j) \right\}$  are equicontinuous. Moreover, they are bounded and defined over a compact set  $\mathcal{X}_p$  and  $\mathcal{X}_w$ . Hence the Arzela–Ascoli theorem [36] implies that, by restricting to a subsequence, there exists uniformly continuous functions  $\hat{f}_{p_j}$  and  $\hat{f}_{w_j}$  such that (40) and (41) in Lemma 3 are satisfied.

Next, we will demonstrate the consistency of gradients of the surrogate function at the limit point. Clearly, according to the quadratic surrogate functions in (16) and (17), we have  $\lim_{i \rightarrow \infty} \mathbf{f}_{p_j}^{(t_i)} = \lim_{i \rightarrow \infty} \nabla_{\mathbf{p}_j} \bar{f}_{p_j}^{(t_i)}(\mathbf{p}_j^{(t_i)})$  and  $\lim_{i \rightarrow \infty} \mathbf{f}_{w_j}^{(t_i)} = \lim_{i \rightarrow \infty} \nabla_{\mathbf{w}_j} \bar{f}_{w_j}^{(t_i)}(\mathbf{w}_j^{(t_i)})$ . And because of (40) and (41), we further have  $\lim_{i \rightarrow \infty} \mathbf{f}_{p_j}^{(t_i)} = \nabla_{\mathbf{p}_j} \hat{f}_{p_j}(\mathbf{p}_j^*)$  and  $\lim_{i \rightarrow \infty} \mathbf{f}_{w_j}^{(t_i)} = \nabla_{\mathbf{w}_j} \hat{f}_{w_j}(\mathbf{w}_j^*)$ . Finally, using Lemma 5, we have

$$\left\| \nabla_{\mathbf{p}_j} \hat{f}_{p_j}(\mathbf{p}_j^*) - \nabla_{\mathbf{p}_j} \mathbf{L}(\mathbf{p}^*, \mathbf{w}^*) \right\| = 0, \quad (51)$$

$$\left\| \nabla_{\mathbf{w}_j} \hat{f}_{w_j}(\mathbf{w}_j^*) - \nabla_{\mathbf{w}_j} \mathbf{L}(\mathbf{p}^*, \mathbf{w}^*) \right\| = 0, \quad (52)$$

almost surely.

## REFERENCES

- [1] F. Liu, Y. Cui, C. Masouros, J. Xu, T. X. Han, Y. C. Eldar, and S. Buzzi, “Integrated sensing and communications: Toward dual-functional wireless networks for 6g and beyond,” *IEEE Journal on Selected Areas in Communications*, vol. 40, no. 6, pp. 1728–1767, 2022.
- [2] M. J. Beal, “Variational algorithms for approximate bayesian inference,” *Phd Thesis University of London*, 2003.
- [3] B. Zhou, Q. Chen, H. Wymeersch, P. Xiao, and L. Zhao, “Variational inference-based positioning with nondeterministic measurement accuracies and reference location errors,” *IEEE Transactions on Mobile Computing*, vol. 16, no. 10, pp. 2955–2969, 2017.
- [4] R. M. Neal, “Probabilistic inference using markov chain monte carlo methods,” 1993.
- [5] A. Doucet, N. De Freitas, N. J. Gordon *et al.*, *Sequential Monte Carlo methods in practice*. Springer, 2001, vol. 1, no. 2.
- [6] B. Zhou and Q. Chen, “On the particle-assisted stochastic search mechanism in wireless cooperative localization,” *IEEE Transactions on Wireless Communications*, vol. 15, no. 7, pp. 4765–4777, 2016.
- [7] Q. Liu and D. Wang, “Stein variational gradient descent: A general purpose bayesian inference algorithm,” *Advances in neural information processing systems*, vol. 29, 2016.
- [8] R. Ranganath, S. Gerrish, and D. Blei, “Black box variational inference,” in *Artificial intelligence and statistics*. PMLR, 2014, pp. 814–822.
- [9] M. S. Arulampalam, S. Maskell, N. Gordon, and T. Clapp, “A tutorial on particle filters for online nonlinear/non-gaussian bayesian tracking,” *IEEE Transactions on signal processing*, vol. 50, no. 2, pp. 174–188, 2002.

- [10] B. Dai, N. He, H. Dai, and L. Song, "Provable bayesian inference via particle mirror descent," in *Artificial Intelligence and Statistics*. PMLR, 2016, pp. 985–994.
- [11] M. D. Hoffman, D. M. Blei, C. Wang, and J. Paisley, "Stochastic variational inference," *Journal of Machine Learning Research*, 2013.
- [12] A. Liu, V. K. N. Lau, and B. Kananian, "Stochastic successive convex approximation for non-convex constrained stochastic optimization," *IEEE Transactions on Signal Processing*, vol. 67, no. 16, pp. 4189–4203, 2019.
- [13] Y. Yang, G. Scutari, D. P. Palomar, and M. Pesavento, "A parallel decomposition method for nonconvex stochastic multi-agent optimization problems," *IEEE Transactions on Signal Processing*, vol. 64, no. 11, pp. 2949–2964, 2016.
- [14] Z. Hu, A. Liu, Y. Wan, T. X. Han, and M. Zhao, "A two-stage multiband radar sensing scheme via stochastic particle-based variational bayesian inference," 2023.
- [15] A. Balatsoukas-Stimming and C. Studer, "Deep unfolding for communications systems: A survey and some new directions," in *2019 IEEE International Workshop on Signal Processing Systems (SiPS)*, 2019, pp. 266–271.
- [16] J. R. Hershey, J. L. Roux, and F. Weninger, "Deep unfolding: Model-based inspiration of novel deep architectures," *Computer Science*, 2014.
- [17] Q. Wan, J. Fang, Y. Huang, H. Duan, and H. Li, "A variational bayesian inference-inspired unrolled deep network for mimo detection," *IEEE Transactions on Signal Processing*, vol. 70, pp. 423–437, 2022.
- [18] Z. Huang, A. Liu, Y. Cai, and M.-J. Zhao, "Deep stochastic optimization for algorithm-specific pilot design in massive mimo," in *2021 IEEE Statistical Signal Processing Workshop (SSP)*, 2021, pp. 191–195.
- [19] Y. Zhang, J. Sun, J. Xue, G. Y. Li, and Z. Xu, "Deep expectation-maximization for joint mimo channel estimation and signal detection," *IEEE Transactions on Signal Processing*, vol. 70, pp. 4483–4497, 2022.
- [20] W. Jin, H. He, C.-K. Wen, S. Jin, and G. Y. Li, "Adaptive channel estimation based on model-driven deep learning for wideband mmwave systems," in *2021 IEEE Global Communications Conference (GLOBECOM)*, 2021, pp. 1–6.
- [21] D. Ha, A. M. Dai, and Q. V. Le, "Hypernetworks," in *International Conference on Learning Representations*, 2017. [Online]. Available: <https://openreview.net/forum?id=rkpACe1lx>
- [22] G. Parisi and R. Shankar, "Statistical field theory," 1988.
- [23] I. Sharp, K. Yu, and T. Sathyan, "Positional accuracy measurement and error modeling for mobile tracking," *IEEE Transactions on Mobile Computing*, vol. 11, no. 6, pp. 1021–1032, 2012.
- [24] M. Vemula, M. F. Bugallo, and P. M. Djuric, "Sensor self-localization with beacon position uncertainty," *Signal Processing*, vol. 89, no. 6, pp. 1144–1154, 2009.
- [25] M. Angelichinoski, D. Denkovski, V. Atanasovski, and L. Gavrilovska, "Cramér–rao lower bounds of rss-based localization with anchor position uncertainty," *IEEE Transactions on Information Theory*, vol. 61, no. 5, pp. 2807–2834, 2015.
- [26] Y. Wan, A. Liu, Q. Hu, M. Zhang, and Y. Cai, "Multiband delay estimation for localization using a two-stage global estimation scheme," *IEEE Transactions on Wireless Communications*, pp. 1–1, 2023.
- [27] P. Pan, Y. Zhang, Z. Deng, and W. Qi, "Deep learning-based 2-d frequency estimation of multiple sinusoids," *IEEE Transactions on Neural Networks and Learning Systems*, vol. 33, no. 10, pp. 5429–5440, 2022.
- [28] E. Jang, S. Gu, and B. Poole, "Categorical reparameterization with gumbel-softmax," *arXiv e-prints*, 2016.
- [29] Y. Chen and X. Ye, "Projection onto a simplex," *arXiv preprint arXiv:1101.6081*, 2011.
- [30] S. Boyd and J. Dattorro, "Alternating projections," *Lecture Notes of Ee O*, 2003.
- [31] D. Kingma and J. Ba, "Adam: A method for stochastic optimization," *International Conference on Learning Representations*, 12 2014.
- [32] Z. Hu, A. Liu, Y. Wan, T. X. Han, and M. Zhao, "A two-stage multiband radar sensing scheme via stochastic particle-based variational bayesian inference," *arXiv preprint arXiv:2207.10427*, 2023.
- [33] Y. Wei, M.-M. Zhao, M. Hong, M.-J. Zhao, and M. Lei, "Learned conjugate gradient descent network for massive mimo detection," *IEEE Transactions on Signal Processing*, vol. 68, pp. 6336–6349, 2020.
- [34] M. Pourkhaatoun and S. A. Zekavat, "High-resolution low-complexity cognitive-radio-based multiband range estimation: Concatenated spectrum vs. fusion-based," *IEEE Systems Journal*, vol. 8, no. 1, pp. 83–92, 2014.
- [35] A. Ruszczyński, "Feasible direction methods for stochastic programming problems," *Mathematical Programming*, vol. 19, no. 1, pp. 220–229, 1980.
- [36] N. Dunford and J. T. Schwartz, "Linear operators: Part I general theory," *Interscience Publishers*, 1988.